Development of a Smart Prosthetic Hand Using Fuzzy Logic for Muscle Signal Interpretation

Qaisar Zia
09-244242-007

A thesis submitted in fulfilment of the requirements for the award of degree of Master of Science (Electrical Engineering)

Department of Electrical Engineering

BAHRIA UNIVERSITY ISLAMABAD

August 2026

MS-14

Approval for Examination

Scholar's Name : **Qaisar Zia**
Registration Number: **70076**
Program of Study: **MS in Electrical Engineering**
Thesis Title: **Development of a Smart Prosthetic Hand Using Fuzzy Logic for Muscle Signal Interpretation**

It is to certify that the above scholar's thesis has been completed to my satisfaction and, to my belief, its standard is appropriate for submission for examination. I have also conducted plagiarism test of this thesis using HEC prescribed software and found similarity index **8**% (excluding self-citation), that is within the permissible limit set by the HEC for the MS degree thesis. I have also found the thesis in a format recognized by the BU for the MS thesis.

Principal Supervisor Signature: ____________________________________

Date:
Name:

Co-Supervisor Signature: ____________________________________

Date:

Name:

MS-14A

Author's Declaration

I, hereby state that my MS thesis titled

" Development of a Smart Prosthetic Hand Using Fuzzy Logic for Muscle Signal Interpretation "

is my own work and has not been submitted previously by me for taking any degree from this university

Bahria University

or anywhere else in the country/world.

At any time if my statement is found to be incorrect even after my graduation, the University has the right to withdraw/cancel my MS degree.

Name of Scholar: **Qaisar Zia**

Date:

MS-14B

Plagiarism Undertaking

I, solemnly declare that research work presented in the thesis titled

"Development of a Smart Prosthetic Hand Using Fuzzy Logic for Muscle Signal Interpretation "

is solely my research work with no significant contribution from any other person. Small contribution / help wherever taken has been duly acknowledged and that complete thesis has been written by me.

I understand the zero tolerance policy of the HEC and Bahria University towards plagiarism. Therefore I as an Author of the above titled thesis declare that no portion of my thesis has been plagiarized and any material used as reference is properly referred / cited.

I undertake that if I am found guilty of any formal plagiarism in the above titled thesis even after award of MS degree, the university reserves the right to withdraw / revoke my MS degree and that HEC and the University has the right to publish my name on the HEC / University website on which names of scholars are placed who submitted plagiarized thesis.

Scholar/Author's Sign: ___________________________

Name of Scholar: **Qaisar Zia**

Acknowledgements

All praise is due to Allah Almighty, the Most Merciful and Most Beneficent, whose countless blessings gave me the strength, patience, and perseverance to complete this work. Without His guidance, none of this would have been possible. I am sincerely thankful to my supervisors, Dr. Maryam Iqbal, for their unwavering guidance, encouragement, and patience throughout this research. From the initial stages of choosing the topic to the final revisions of this thesis, their feedback kept the work moving in the right direction. Their readiness to make time for meetings, even at short notice, and their emphasis on clarity and rigour have profoundly influenced both this thesis and my development as a researcher. I could not have wished for more supportive supervisors. I extend my sincere thanks to the faculty of the Department of Electrical Engineering, Bahria University Islamabad, whose teaching during my coursework built the foundation on which this research stands. I am equally thankful to the administrative and laboratory staff for their cooperation and for providing a supportive academic environment and the resources needed for this work.

I am also grateful to my seniors and fellow postgraduate students in the department for their company, discussions, and moral support during the course of this degree. Their willingness to share their experiences and offer advice made the more difficult stretches of this journey easier to bear. I would like to thank my friends outside the university as well, who showed patience and understanding during the long periods when this work demanded all of my time and attention. Finally, I owe my deepest gratitude to my family. To my parents, whose prayers have accompanied me at every step of my life, and whose sacrifices made my education possible, no words of thanks can ever be enough. To my siblings, thank you for your constant encouragement and for believing in me even when I doubted myself. This achievement belongs to all of you as much as it does to me.

Engr. Qaisar Zia
Bahria University, Islamabad 2026

Abstract

The thumb contributes roughly half of the total functional capacity of the human hand, since opposition and pinch are governed by its motion across the carpometacarpal (CMC) saddle joint. Restoring credible thumb motion to a powered prosthesis is therefore central to restoring credible hand function, and the difficulty lies in the controller rather than the mechanism. The inertial, damping and elastic parameters of the CMC joint are not known with certainty, and the controller driving it must remain accurate under that uncertainty. A fixed gain controller tuned to nominal values loses performance when the true parameters drift, and a conventional fuzzy controller with a static rule base cannot adapt to a plant it did not see during design. This thesis examines whether an adaptive fuzzy logic controller with a Lyapunov based online update law can track a commanded angular trajectory of the thumb CMC joint on a plant whose dynamics are not exactly known in advance.

The study is carried out entirely in simulation in MATLAB R2025b and Simulink. The joint is modelled as a single degree of freedom in flexion extension, driven by a smooth trajectory generated from a sigmoid command through a critically damped reference model. An adaptive Takagi Sugeno Kang fuzzy controller with twelve Gaussian basis functions on the joint state produces an online estimate of the plant nonlinearity. That estimate is combined with sliding mode feedback in a certainty equivalent control law and updated by a Lyapunov derived adaptation law with bounded parameters, with convergence of the tracking error following from Barbalat's lemma.

The controller is evaluated across twelve simulation cases spanning six reference amplitudes from 0.20 to 1.05 radians, four levels of plant parameter uncertainty, four load disturbance magnitudes and four reference trajectory types. Each case is run against a non adaptive equivalent differing only in the adaptation gain, isolating what adaptation contributes. Without adaptation the joint settles 8.57 per cent short of its commanded angle at every setpoint and never enters the two per cent settling band. With adaptation the steady state error falls to 0.03 per cent, tracking error is reduced by 41.9 per cent on the nominal plant, and the advantage widens to 54.8 per cent when the plant parameters are doubled. On a continuously periodic reference, where no steady state offset exists for the adaptation to remove, the benefit falls to 2.2 percent.

The contribution of the work is the design, stability analysis and simulation based validation of an adaptive TSK fuzzy controller for the thumb CMC joint, together with quantitative evidence that Lyapunov based online adaptation eliminates the steady state error that fixed gain sliding mode feedback cannot remove. The results establish the feasibility of the proposed approach for position control of an uncertain prosthetic joint.

Keywords: Adaptive fuzzy control, Takagi Sugeno Kang (TSK) fuzzy system, Lyapunov based parameter adaptation, thumb carpometacarpal (CMC) joint, prosthetic hand, sliding surface, MATLAB simulation, uncertain nonlinear dynamics.

TABLE OF CONTENTS

LIST OF TABLE

LIST OF FIGURE

ACRONYMS AND ABBREVIATIONS

CNS	Central Nervous System
DP	Distal Phalenge
IP	Intermediate Phalange
PP	Proximal Phalange EOMs Equations Of Motions
EMG	ElectroMyoGraphic Signal IMU Inertial Measurement Unit
SS	State Space
PIP	Proximal InterPhalangeal
DIP	Distal InterPhalangeal
MCP	MetaCarpoPhalangeal
FLC	Fuzzy Logic Controller
SMC-FLC	Sliding Mode Control- Fuzzy Logic Controller
DOF	Degree Of Freedom
FIS	Fuzzy Inference System
AMD	Active Mass Dampers

CHAPTER 1

INTRODUCTION

1.1 Introduction

The loss of a hand means the loss of one of the most versatile instruments the human body has, and recovering even part of its function remains an open problem in rehabilitation engineering. A powered prosthesis must do three things in quick succession and within a few tens of milliseconds: read the user's intention, decide how to move, and drive its actuators so that the motion is both accurate and smooth. The actuators and sensors needed have matured, and the limiting factor is no longer the mechanism but the control law that governs it [1]. This thesis deals with that control law.

The clinical need is constant. Loss of the upper limb, through trauma, disease, or a congenital condition, removes a person's primary tool for manipulating the physical world, and restoring even basic grasping produces measurable improvements in daily independence. That benefit exists only if the device is worn. High abandonment rates for powered hands are frequently attributed to control that feels unnatural and tiring to operate. The goal of a prosthetic controller is therefore not simply to move a joint to a commanded angle but to do so in a manner the user perceives as predictable and smooth, since those qualities determine whether the device is integrated into daily life or left in a drawer [2].

Prosthetic control has moved through several phases toward that goal. Early body-powered hands used cables and harnesses to translate shoulder movement into grip: simple and reliable, but only loosely coupled to what the user intended. Myoelectric control replaced the mechanical link with an electrical one, reading the activity of residual muscles and bringing the command closer to actual intent [3]. Controllers then grew in capability, from on-off switching to proportional control and, more recently, to pattern-recognition systems that identify intended gestures. Intent estimation has improved at each stage, but one problem has persisted: the command is derived from a noisy and variable biological signal, and the joint it drives has parameters that are not exactly known. Recent reviews confirm that the outstanding difficulty has moved from the mechanical layer to the control layer [4, 5].

The last five years have seen substantial research activity aimed at that gap, and it is worth locating the present thesis within that landscape. Four themes dominate the recent literature. The first is the application of deep learning to electromyographic decoding, in which convolutional and recurrent networks map raw or lightly processed signals to intended grasps with accuracies exceeding hand-designed features on classification benchmarks [6–8]. The second is the integration of intelligent control with modern prosthetic hardware, ranging from underactuated compliant hands whose grasp force is regulated through stiffness estimates [9] to research prostheses in which sensing, mechanics and control are co-designed as a single system [5]. The third is the emergence of adaptive and hybrid fuzzy controllers for prosthetic and rehabilitation devices, including real-time adaptive backstepping controllers enhanced by fuzzy approximation for multi-degree-of-freedom prosthetic hands [10], fuzzy adaptive controllers for hand rehabilitation robots at scales relevant to prosthetic joints [11], fuzzy control strategies for lower-limb rehabilitation exoskeletons [12], and connected fuzzy rehabilitation systems for home use [13]. The fourth is the movement toward multimodal sensing, in which electromyography is combined with force, vision or inertial signals so that the controller has richer information about both intent and context, with recent reviews identifying the closed-loop controller that consumes these signals as the outstanding open problem [14].

These four themes situate the present work. It does not advance deep-learning-based intent decoding, nor does it contribute to sensor fusion. It engages with the third theme,adaptive fuzzy control for prosthetic hardware, and does so at a specific anatomical site, the thumb carpometacarpal joint, which the recent literature has not substantively addressed.

The hand the prosthesis imitates is a structure of considerable mechanical subtlety, containing twenty-seven bones and roughly twenty-three degrees of freedom at joints that move in graded, coordinated ways [15]. The four fingers each have three joints: the metacarpophalangeal, proximal interphalangeal, and distal interphalangeal. The interphalangeal joints flex and extend about a single axis, while the metacarpophalangeal joint permits a second axis of abduction. This kinematic arrangement and the angular convention used throughout the thesis are shown in Figure 1.1.

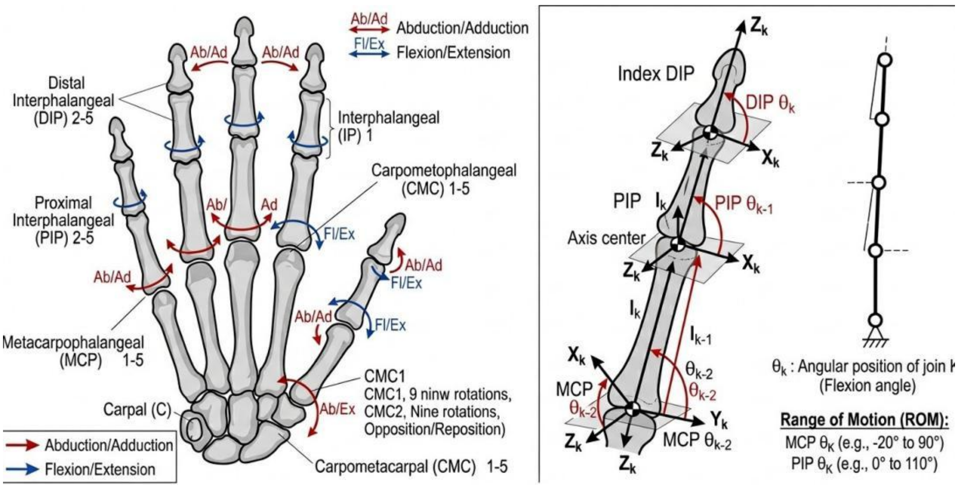

Figure 1.1: Kinematic joints of the human hand model.

It contributes roughly half the total functional capacity of the hand [16], because opposition and pinch, the two motions that make grasping possible, are governed by its motion across the carpometacarpal saddle joint. A prosthetic hand that reproduces finger flexion faithfully but cannot position its thumb accurately restores far less function than the count of actuated joints would suggest. The carpometacarpal joint is therefore the site at which control accuracy matters most, and it is the site addressed here.

What matters to a controller at any one joint is its angle and how that angle changes over time. A single joint is therefore a meaningful unit of study even within so rich a structure, and the carpometacarpal joint is the one whose accurate control contributes most to restored function.

The difficulty at that joint lies in the plant rather than in the mechanism. The joint is small, and its inertia, damping and elastic restoring stiffness are not known with certainty. They depend on assembly tolerance, wear, temperature and the mechanical coupling to the individual user, and they change over the life of the device. A controller tuned to nominal parameter values loses performance when the true parameters differ, and the conventional response, a proportional-integral-derivative law, assumes a linear plant with known parameters and reduces the control decision to a fixed weighted sum of the error and its integral and derivative [17]. Bench tuning that works for one set of parameters rarely transfers cleanly to another. The gap is clear: the problem is nonlinear and uncertain, while the conventional controller is neither.

Fuzzy logic provides a formal response to that gap. A fuzzy inference system, proposed by Zadeh and developed for control by Mamdani and Assilian, maps inputs to outputs through linguistic rules rather than a single algebraic gain [18, 19]. Membership functions describe the degree to which a measured value belongs to sets such as "negative," "zero," or "large positive," and a rule base encodes how an expert would respond to each combination of conditions. The present work uses the Takagi-Sugeno-Kang formulation, in which rule consequents are functions of the input rather than fuzzy sets. That distinction is what makes online adaptation tractable: the consequent parameters enter the control law linearly, so an update law for them can be derived from a Lyapunov function and their boundedness established analytically. Recent adaptive fuzzy control research has developed this line into schemes offering finite-time convergence guarantees [17] and event-triggered updates suitable for embedded deployment [20], and the present thesis builds on it.

The study is carried out in simulation. This follows from the question asked rather than from convenience. Simulation makes it possible to vary the control strategy alone while holding the plant model, the reference signals, and the disturbance conditions exactly constant, which no physical test bench permits. Every experiment is reproducible, and internal quantities such as the adaptive parameter vector and the sliding variable are directly accessible, whereas a physical rig could observe them only by adding sensors that introduce error of their own. The work is implemented in MATLAB R2025b and Simulink.

On this basis the thesis develops and evaluates an adaptive Takagi-Sugeno-Kang fuzzy controller for the thumb carpometacarpal joint. The dynamic model of the joint in flexion-extension is derived from first principles. A sliding surface reduces the second-order tracking problem to a first-order stable dynamic, and a certainty-equivalent control law combines sliding-mode feedback with an online fuzzy estimate of the plant nonlinearity constructed from twelve Gaussian basis functions on the joint state. The estimate is updated by a Lyapunov-derived adaptation law, and closed-loop stability is established analytically before any simulation is run.

The controller is evaluated against a non-adaptive equivalent obtained by setting the adaptation gain to zero. That benchmark shares the basis functions, the sliding surface, the feedback gains and the parameter bounds with the proposed controller, so any difference in performance is attributable to adaptation alone. This is a stronger comparison than one against a structurally different controller, where differences could arise from any of several sources at once.

A note on scope is warranted. The title of this thesis names the broader system: a smart prosthetic hand using fuzzy logic for muscle signal interpretation. Such a system has two layers. The first estimates the user's intended motion from the electromyographic signal and converts it into a commanded joint trajectory. The second drives the joint to follow that trajectory on hardware whose parameters are not exactly known. The recent literature reviewed in Chapter 2 has invested heavily in the first layer through pattern-recognition and deep-learning approaches to intent estimation and comparatively little in the second, which several of the works surveyed identify as the outstanding open problem.

This thesis addresses the second layer. The reference trajectory is generated internally rather than derived from a measured electromyographic signal, which isolates the closed-loop controller from intent-estimation error and allows the contribution of the control law to be measured without confounding. The fuzzy logic named in the title is applied to the interpretation of the plant rather than of the muscle signal: the Takagi-Sugeno-Kang system estimates the unknown joint dynamics online, and the linguistic structure of the fuzzy rule base is retained in the labelling of the basis function centers. Integration with a myoelectric front-end is identified as future work in Chapter 5, and is the step that would join the layer developed here to the layer the title's phrase describes.

1.2 Problem Statement and Motivation

This work is motivated by a mismatch between the promise of powered prostheses and their actual behaviour. A user who has lost a hand wants a device that moves where it is told, when it is told, without the hesitation or jerk that makes the device feel foreign. The hardware exists to generate that response. What remains unsolved is the control law that converts a commanded position into motion the user recognises as their own. Conventional controllers use fixed linear mappings for that step, and the resulting unnatural feel is a primary reason powered hands are abandoned rather than worn [3].

The difficulty lies in the plant. The thumb carpometacarpal joint has uncertain inertia, damping and elastic stiffness, and its behaviour is not strictly linear. The usual choice, a proportional-integral-derivative controller, assumes both difficulties away: the plant is treated as linear with known parameters, and the control decision collapses into a fixed weighted sum of the error and its integral and derivative [17]. A tuning that answers one operating condition fails in another, and the resulting motion is either sluggish or unsteady. The control problem is both nonlinear and uncertain, so a fixed linear control law is inherently inappropriate for addressing it. There is a further difficulty specific to sliding-mode feedback, and it is the one this thesis addresses directly. Sliding-mode control generates actuator torque in proportion to the tracking error. Holding a joint at a commanded angle against its elastic restoring torque therefore requires a persistent error to sustain the necessary control effort. Such a controller cannot reach its target exactly, however well its gains are chosen, because the error is the mechanism by which the torque is produced. An adaptive term that learns the required holding torque and supplies it

independently of the instantaneous error removes that constraint, and quantifying what it removes is the object of this study.
The problem is framed as one question: can an adaptive fuzzy logic controller with a Lyapunov based online update law track a commanded angular trajectory of the thumb carpometacarpal joint on a plant whose inertial, damping and elastic parameters are not exactly known, To answer it on fair terms, the study fixes the carpometacarpal joint in flexion extension as the plant, derives its dynamics from first principles, and generates the reference trajectory through a critically damped reference model so that the commanded motion is itself dynamically achievable. The adaptive controller is then compared against a non-adaptive equivalent differing only in the adaptation gain, across reference amplitudes spanning the joint's operating range, levels of plant parameter uncertainty, load disturbance magnitudes and reference trajectory types. A consistent improvement across those conditions would demonstrate that online adaptation addresses the uncertainty a fixed-parameter controller structurally cannot.

1.3 Research Objectives

- To derive from first principles the dynamic model of the thumb carpometacarpal joint in flexion–extension, and to express it in transfer-function and state-space form with parameter values representative of the human joint.
- To design an adaptive Takagi–Sugeno–Kang fuzzy controller for that joint, in which twelve Gaussian basis functions on the joint state produce an online estimate of the plant nonlinearity, combined with sliding-mode feedback through a certainty-equivalent control law.
- To derive the parameter adaptation law from a Lyapunov function that bounds both the tracking error and the parameter estimation error, and to establish boundedness of all closed-loop signals together with convergence of the tracking error to zero.
- To justify each controller design parameter, distinguishing those derived from the reference-model dynamics from those obtained by empirical sweep, and to state the criterion applied in each case.
- To implement the controller in MATLAB R2025b and Simulink, and to validate the plant implementation against its analytical model at multiple independent operating points.
- To evaluate the controller against a non-adaptive equivalent differing only in the adaptation gain, across reference amplitudes spanning the joint's operating range, levels of plant parameter uncertainty, load disturbance magnitudes, reference trajectory types and measurement noise conditions.
- To quantify the contribution of online adaptation using root-mean-square error, integral absolute error, integral squared error, rise time, settling time, overshoot and steady-state accuracy, and to identify the conditions under which that contribution is largest and smallest.

1.4 Limitations

The scope of this study carries the following limitations.

- The work is carried out entirely in software. No physical prosthesis is constructed and no experimental validation on hardware is performed. The results establish feasibility in simulation and do not by themselves establish performance on a physical device.
- The mechanical model is restricted to the flexion–extension axis of the thumb carpometacarpal joint. The abduction–adduction axis of the same joint, the metacarpophalangeal and interphalangeal joints of the thumb, and coupling between the thumb and the fingers are outside the present scope.
- The reference trajectory is generated internally through a reference model rather than derived from a measured electromyographic signal. Uncertainty entering through the reference channel is therefore not modelled, and the study isolates the closed-loop controller from intent-estimation error.
- The primary comparison is against a non-adaptive equivalent of the proposed controller, which isolates the contribution of adaptation. Comparison against conventional alternatives, including proportional-integral-derivative and Mamdani fuzzy controllers, is presented in Chapter4 but was not the principal object of the study.
- Actuator dynamics, torque saturation, sensor latency and quantisation are not represented in the plant model. Measurement noise is examined separately in Chapter4, but the stability analysis of Chapter3 applies to the noise-free case.
- Factors governing clinical adoption, including long-term reliability, user training and regulatory approval, lie beyond the scope of a simulation study and are acknowledged but not addressed.

1.5 Thesis Organisation

The thesis is divided into five chapters. This chapter has presented the problem of controlling an uncertain prosthetic joint, outlined the motivation and research question, and defined the aims and constraints of the study.
Chapter 2 surveys five strands of scholarship that intersect with the research question: the theoretical underpinnings of adaptive fuzzy control, its recent developments in finite-time and event-triggered settings, the traditional prosthetic hand control literature, the rehabilitation robotics literature, and contemporary machine-learning work on prosthetic control. It then delineates the remaining research gap following these prior contributions.
Chapter 3 presents the methodology. It derives the dynamic model of the thumb carpometacarpal joint, specifies the reference model, the sliding surface and the certainty-equivalent control law, constructs the fuzzy estimate from twelve Gaussian basis functions, derives the adaptation law from a Lyapunov function, and establishes closed-loop stability. It closes by justifying each design parameter and enumerating the assumptions on which the analysis rests.

Chapter 4 presents the Simulink implementation and the simulation study. It describes the model architecture subsystem by subsystem, validates the plant against its analytical model, and reports twelve test cases covering reference amplitude, plant parameter uncertainty, load disturbance, reference trajectory type and measurement noise, each compared against the non-adaptive benchmark.

Chapter 5 draws conclusions from the results, states what the study establishes and what it does not, and identifies directions for further work including experimental validation, extension to the coupled multi-joint case, and integration with electromyographic intent estimation.

CHAPTER 2

LITERATURE REVIEW

2.1 Introduction

This chapter examines the literature that this thesis builds on. It is a critical rather than descriptive review: for each work considered, the contribution is identified, the reasoning behind the authors' methodological choices is explained where it matters for interpretation, the limitations that the authors themselves acknowledge or that follow from their methods are stated, and the specific research gap that remains after their contribution is made explicit.

The chapter is organized thematically rather than chronologically. The research question of this thesis whether an adaptive fuzzy logic controller with Lyapunov-based online adaptation can accurately track a commanded angular trajectory of the thumb carpometacarpal joint on a plant whose dynamics are not exactly known sits at the intersection of five distinct bodies of work. The first is the theoretical foundation of adaptive fuzzy control, developed principally between 1965 and 2003. The second is the recent extension of that theory to modern requirements such as finite-time convergence, event-triggered updates, and fault tolerance. The third is the classical prosthetic hand control literature, which has focused on classifying user intent from surface electromyography rather than on continuous joint control. The fourth is the rehabilitation-robotics literature, which has recently begun to apply adaptive fuzzy methods to upper- and lower-limb prostheses and exoskeletons but has not converged on the thumb specifically. The fifth is the modern machine-learning literature on prosthetic control, which has advanced significantly on the classification problem but has left the closed-loop control problem largely open.

The gap that motivates this thesis becomes visible only when these five streams are read against one another, which is why this chapter is organised as it is. Each section addresses one stream, evaluates its contributions and shortcomings in the context of the present work, and connects it to the next stream.

2.2 Theoretical Foundations of Fuzzy and Adaptive Fuzzy Control

The theoretical foundations of adaptive fuzzy control have developed over four decades and remain the mathematical bedrock on which every application of the technique rests, including the one developed in this thesis. Understanding the sequence in which the theory developed is essential for placing the present work correctly.

Zadeh [1] introduced the theory of fuzzy sets in 1965 as a response to a specific limitation of classical set theory: the inability to represent gradual, continuous transitions between categories such as “warm” and “hot” or “close to the target” and “far from the target”. His contribution was the formalisation of graded membership through the membership function, which assigns to each element of a universe of discourse a real number in the interval $[0, 1]$ representing its degree of belonging to the set. The strength of the work, viewed from six decades later, is the mathematical rigour with which he showed that fuzzy sets could be manipulated using operations analogous to those of classical set theory, which laid the foundation for every subsequent application. Its limitation, from the perspective of prosthetic control, is that the work is purely mathematical and offers no guidance on how a fuzzy system should be embedded in a feedback loop nor how the resulting closed-loop system should be shown to be stable. Zadeh himself did not treat fuzzy sets as a control-engineering tool; that step was taken a decade later by Mamdani.

The transition from Zadeh’s theory to a working controller was made by Mamdani and Assilian [2] in 1975, who addressed the practical question of whether a plant without an explicit mathematical model could be regulated using operator knowledge rendered as fuzzy rules. They chose a steam engine as their test bed because it exhibited nonlinear dynamics that classical PID control handled poorly and because operator experience was rich and articulate. Their contribution is the linguistic rule-base architecture the “if error is negative and change in error is negative, then control is positive” structure that is still called the Mamdani inference model. The strength of the work is the demonstration that expert reasoning about control could be encoded formally and used to close a loop.

Its weakness, in the context of the present thesis, is subtle but fundamental: the rule base is static. Once designed, it cannot adjust to a plant whose parameters differ from those the designer had in mind. This mattered less in Mamdani and Assilian’s application, where a single steam engine had reasonably repeatable dynamics, but it matters enormously in prosthetic control, where the mechanical parameters of a joint drift between users, between sessions with the same user, and even within a single session as fatigue accumulates. A fixed rule base can be redesigned each time these parameters change, but the redesign requires a designer, and the whole point of a prosthetic controller is that it must operate autonomously in the user’s daily life without such intervention. The gap that Mamdani-style control leaves open, therefore, is precisely the need for a controller that adapts its parameters online, a gap that Wang and Zak later closed.

Takagi et al [3] proposed a decade later, in 1985, an alternative architecture that would prove more amenable to online adaptation. The Mamdani model represents each rule’s output as a linguistic label (for example “positive small”) that must be defuzzified through a centroid or maximum operation to produce a crisp control signal. Takagi and Sugeno replaced the linguistic output with a functional consequent, typically a linear combination of the input variables so that each rule outputs a real number directly. This apparently minor change has two consequences that matter for adaptive control. First, the output is differentiable with respect to the rule parameters, which makes gradient-based tuning of those parameters possible in a way that is awkward for Mamdani systems.Second, the resulting fuzzy system can be interpreted mathematically as a universal function approximator, meaning that a Takagi Sugeno Kang system with sufficient rules can approximate any continuous function on a compact domain to arbitrary accuracy. Both properties are essential for the certainty-equivalent adaptive control law used in the present thesis, where the fuzzy system must approximate an unknown plant nonlinearity and its parameters must be updated online by a Lyapunov-derived rule.

The weakness of the original Takagi Sugeno work, as they themselves acknowledged, is the absence of stability guarantees when the parameters are updated online. Their 1985 paper established the architecture but treated the parameters as fixed after tuning. This was the barrier to using the Takagi Sugeno Kang architecture in safety-critical applications for the next eight years, until Wang's 1993 paper provided the missing stability analysis.

Wang et al [4] gave the first systematic treatment of adaptive fuzzy control with a Lyapunov-based analysis in 1993, with a fuller exposition in his 1994 book. His contribution converts fuzzy control from an ad hoc engineering technique into a rigorous nonlinear control method with formal convergence guarantees. The strength of Wang's framework is threefold. First, it applies to a broad class of nonlinear plants those that can be written in a strict feedback form with a matched uncertainty structure which covers most single-input single-output mechanical systems including the thumb CMC joint of this thesis. Second, it provides the closed-loop stability proof that the earlier Takagi Sugeno papers lacked, using a Lyapunov function that bounds both the tracking error and the parameter estimation error simultaneously. Third, and most importantly for the present work, it establishes the certainty-equivalent control law $u = J(\hat{f} + \ddot{x}_d + K_p e + K_d \dot{e})$ that the thesis adopts, in which the fuzzy system's estimate $\hat{f}$ of the plant nonlinearity substitutes for the true nonlinearity as if the estimate were certain.

Its limitation, from the standpoint of the present thesis, is that Wang treats the plant abstractly. His theorems assume that the plant belongs to a class defined by structural properties (relative degree, matched uncertainty, growth conditions) but do not specify numerical values for the plant parameters. The transfer of his framework to a physical system requires the designer to specify the plant inertia, damping, and stiffness; the placement of the basis functions in the state space; the adaptation gain; and the saturation limits none of which Wang's general theory prescribes. Every application of Wang's framework since 1993 has had to make these choices independently, and the choices are what determine whether the resulting controller works well or poorly in practice. The present thesis makes these choices explicitly for the thumb CMC plant in Chapter 3 and defends them in Section 3.5.4.

Zak et al [5] developed the adaptive fuzzy controller in a control-textbook form in 2003 that combines the sliding surface, the certainty-equivalent control law, and the parameter adaptation into a single design procedure suitable for pedagogical exposition and application transfer. Chapter 8 Example 8.15 of Zak's text is the specific framework this thesis adapts. Its strength, relative to Wang's more general treatment, is that the derivation is complete and self-contained: it opens with the equation of motion, defines the sliding surface $\sigma = \lambda e + \dot{e}$, derives the control law by requiring $\dot{\sigma} = 0$ under the certainty-equivalent assumption, and closes with the Barbalat-based convergence argument that shows the tracking error tends to zero as time tends to infinity. A graduate student can follow the derivation end-to-end in a single reading, which is unusual for adaptive control literature. Its limitation is that the worked example is for a generic second-order plant with unit inertia and damping, and it gives no guidance on how the parameters λ , γ_{eff}, and the saturation bound generalize to a plant with the small inertia and low stiffness characteristic of a prosthetic joint. This transfer the numerical instantiation of the Zak framework for the thumb CMC parameters $J = 8 \times 10^{-4}$, $B = 4 \times 10^{-3}$, $K = 3 \times 10^{-2}$ is what Chapter 3 of this thesis carries out.

2.3 Recent Extensions of Adaptive Fuzzy Control

The theoretical foundations above have been extended significantly in the last five years, primarily in response to three practical demands that were not fully addressed by the classical framework: the need for finite-time rather than asymptotic convergence, the need to reduce the computational cost of continuous parameter updates for embedded deployment, and the need to handle actuator faults and other unexpected disturbances gracefully. These extensions are not directly applied in the present thesis, but they define the current frontier of the field and clarify what the present work does and does not contribute to it.

Wang et al [6] developed an adaptive fuzzy finite-time controller for nonlinear systems with actuator faults in 2020. The community's motivation for pursuing finite-time control is the recognition that the classical Lyapunov guarantee that the tracking error tends to zero as time tends to infinity is often insufficient for practical applications where an explicit bound on the settling time is required. Their contribution is a Lyapunov analysis that yields not merely asymptotic convergence but convergence within a computable finite time, together with a mechanism for compensating actuator faults through the fuzzy approximator itself.

The strength of their work is the mathematical elegance of the finite-time analysis and its practical relevance to safety-critical systems that must recover from actuator degradation within a bounded time. Its limitation, for the present thesis, is that the finite-time formulation requires a class-K_∞ growth condition on the Lyapunov function derivative that is not naturally satisfied by the small-inertia thumb CMC plant, and the actuator-fault model they consider does not map onto the parameter-drift model that motivates the present thesis. Their fault model treats faults as sudden, discrete events (a motor becoming stuck at a nonzero torque, for example), whereas the parameter drift this thesis addresses is a continuous, slow variation in the plant's inertial, damping, and stiffness parameters. The two problems require different adaptation architectures, and the finite-time framework is not the natural fit for the present application. It remains, however, a promising direction for future extension of this work when actuator-fault tolerance becomes a design requirement.

Cao et al [7] proposed an observer-based event-triggered adaptive decentralized fuzzy controller for large-scale nonlinear systems in 2021. The community's motivation for event-triggered control is the observation that the classical Lyapunov-based adaptation laws update the parameters continuously at every instant of time even when the tracking error is small and the update is barely changing the parameter values. This continuous updating imposes a computational cost that becomes significant when the controller must be deployed on an embedded processor with limited resources, which is exactly the situation of a wearable prosthetic hand.

Their contribution is to show that event-triggered adaptation, where the parameters are only updated when a given triggering condition is met, can substantially lower this computational cost without sacrificing the stability guaranty. The strength of their work is the rigorous proof that the triggering condition preserves the Lyapunov argument and hence the closed-loop stability, together with quantitative estimates of the computational saving. Its limitation, in the context of the present thesis, is that the decentralized architecture is designed for large-scale interconnected systems with multiple subsystems that communicate over a shared network and does not apply to a single-joint controller of the kind developed here. The event-triggered mechanism itself, however, does apply, and it indicates a promising direction for future extension of the present controller to a multi-joint prosthetic hand where computational cost across all joints becomes a binding constraint. Taken together, [6] and [7] show that the classical Lyapunov framework of Wang and Zak remains under active development and that the field is not settled. The present thesis contributes at a different level: rather than extending the framework, it applies the existing framework to a specific and previously unaddressed plant.

2.4 Classical Prosthetic Hand Control

The theoretical foundations above developed in parallel with, but largely independently of, the prosthetic hand control literature. The prosthetic literature has been driven by a different set of concerns recognising user intent from noisy biological signals, integrating multiple degrees of freedom into anthropomorphic mechanisms, and delivering natural-feeling motion and its dominant paradigm has been classification of intent rather than continuous control of motion.

Hudgins et al [8] published the paper that established the classification paradigm in 1993. Their motivation was the practical observation that surface electromyographic signals recorded from the residual muscles of an amputee contained more information than the simple threshold-based schemes of the time were extracting from them. They introduced a set of time-domain features mean absolute value, zero crossings, slope-sign changes, and waveform length computed over short EMG windows and showed that a small linear classifier trained on these features could distinguish four intended hand motions with high accuracy. The strength of their contribution is enormous: their feature set remains among the most widely used in myoelectric control today, and their paper defined the methodological template that dozens of subsequent studies would follow.

The weakness of their work, from the control perspective this thesis takes, is not a defect in what they did but a consequence of the framing they chose. The output of their system is a discrete class label that indexes one of a small number of preset motions. This means, in a modern prosthetic hand, that the user can command the hand to close, open, rotate, or grasp but cannot command the hand to move a specific finger to a specific angle at a specific speed. Every subsequent paper in the classification tradition inherits this limitation. The result is that prosthetic motion, as delivered by classification-based control, is restricted to a fixed set of stereotyped patterns rather than the continuous, graded motion of a natural hand. The gap this classification framing leaves open is precisely the continuous joint-level control that the present thesis develops.

Castellini et al [9] examined surface EMG in advanced hand prosthetics in an analytical paper in 2009. Their motivation was the observation that increasing sophistication of EMG-based classifiers had not translated into commensurately increasing reliability in real-world use. They identified a robustness-versus-complexity trade-off that continues to hold: as controllers become more sophisticated, they typically become more sensitive to the exact conditions under which they were trained. Small changes in electrode placement, muscle fatigue, or user posture that would leave a simple threshold classifier unaffected can degrade the performance of a sophisticated pattern-recognition system substantially. The strength of their argument is that it explains why decades of steady classifier improvement have not produced a corresponding steady improvement in prosthetic usability. Their claim that structured, rule-based approaches are likely to behave better than purely data-driven approaches when training data is limited supports the choice of fuzzy control in the present thesis, since a fuzzy controller encodes prior knowledge about the control task in its rule base rather than requiring the system to infer that knowledge from data. The limitation of their work is that they do not themselves design or evaluate such a controller; the paper is analytical rather than constructive, and the research gap it identifies the need for structured controllers that combine adaptivity with robustness is precisely the one that the present thesis addresses.

Belter et al [10] reviewed the mechanical design and performance of anthropomorphic prosthetic hands in 2013, at a moment when the field was transitioning from hooks and single-degree-of-freedom grippers to sophisticated multi-fingered hands. They surveyed the mechanisms then available, catalogued their weight, degrees of freedom, and grip patterns, and compared them systematically. The important conclusion they reached, one that this thesis takes seriously, is that the mechanical capability of available devices had already outpaced the controllers that drive them. Sophisticated hands were being built that their control layers could not exploit. This finding motivates the present work directly: the bottleneck in prosthetic hand performance has moved from the mechanical layer to the control layer, and improving the controller is now the intervention with the highest return. The limitation of their work, as a review, is that it identifies the control layer as the bottleneck but does not explicitly advocate or evaluate a controller. Their contribution is diagnostic rather than therapeutic. The research gap they open is one that many subsequent papers, including the present thesis, have attempted to fill from different angles.

Piazza et al [11] deliver the most comprehensive modern survey of prosthetic and robotic hand development. Their motivation was the recognition that the field had matured to the point where a comprehensive taxonomy was overdue. Their strength is the systematic classification of hand designs along the axes of degrees of freedom, actuation, sensing, and control, and the resulting identification of the recurring gap between mechanical ambition and control competence. Along nearly every axis they consider, they identify a trend in which mechanical designs have grown more capable while control designs have grown incrementally at best. Its limitation, for the present thesis, is that as a survey it does not itself develop a controller. Its role in this chapter is to provide the contextual framing within which a single-joint adaptive controller of the kind developed here fits and to establish that the intervention the present thesis makes improving the joint-level controller is one that the field has already identified as necessary.

2.5 Adaptive and Fuzzy Control in Rehabilitation Robotics

The most recent and directly relevant literature combines adaptive or fuzzy control with rehabilitation robotics, and these works are the closest neighbors to the present thesis. The community that produced these papers works at the intersection of control theory and clinical rehabilitation, and its papers typically report the design of a specific controller, its stability analysis, and its evaluation on a particular device intended for a particular clinical purpose. Reading these papers together clarifies both what has been accomplished and what remains open for the thumb specifically.

Yang and colleagues [12] developed a real-time adaptive backstepping controller enhanced by fuzzy approximation for a multi-degree-of-freedom prosthetic hand. Their motivation was the recognition that backstepping a systematic recursive procedure for stabilizing cascaded nonlinear systems could be combined with a fuzzy universal approximator to yield a controller that handled the coupled dynamics of a multi-jointed hand without requiring an explicit model of every joint interaction. The strength of their work is that it demonstrates the practical benefit of combining a rigorous nonlinear control method with a fuzzy approximator for the specific challenge of a multi-jointed prosthetic hand, and it establishes that this combination can operate at real-time rates on a modern embedded processor.

Its limitations, from the perspective of this thesis, are three. First, the controller is applied to the whole hand as a coupled system rather than to any individual joint, which means that the tuning of the controller is entangled with the interaction dynamics of adjacent joints. Isolating a single joint for detailed study, as the present thesis does for the thumb CMC allows a cleaner Lyapunov analysis and more transparent tuning. Second, the backstepping formulation used there differs mathematically from the sliding-surface formulation used here. Backstepping stabilizes the closed loop by constructing a chain of virtual controls, each of which stabilizes one integrator in the cascade; the sliding-surface approach used here collapses the tracking problem to a single first-order stable dynamic in the sliding variable and does not require the recursive cascade construction. The two formulations are complementary rather than competing, and the choice between them is driven by the plant structure. For the second-order thumb CMC plant, the sliding-surface formulation is the more natural choice. Third, the thumb CMC joint in particular is not called out as a distinct control problem in Yang's paper. The present thesis complements this work by focusing precisely on the thumb CMC joint and by using the Zak sliding-surface framework rather than backstepping.

Zhou and colleagues [13] proposed an optimal fuzzy logic-based control strategy for a lower-limb rehabilitation exoskeleton. Their motivation was the recurring frustration in fuzzy control practice that the parameters of a fuzzy controller, the rules, the membership function shapes and centers, and the scaling factors are typically chosen by hand, which is time-consuming and does not guarantee that the chosen parameters are near-optimal for the plant at hand. Their contribution is a systematic method for tuning these parameters by optimisation, using a cost function that combines tracking accuracy with control effort. The strength of their work is that it addresses one of the recurring weaknesses of classical fuzzy control head-on, and it demonstrates quantitative improvement over hand-tuned controllers on the same exoskeleton.

Its drawback, for the present thesis, is that the application is a lower-limb exoskeleton with substantially larger inertias and stiffnesses than those of the thumb joints. A hip joint has an inertia several orders of magnitude larger than the thumb carpometacarpal joint, and this scale difference means that the numerical values of the optimised parameters do not transfer directly. It is not evident how the optimisation procedure would generalise to the low-inertia regime of a prosthetic thumb without substantial reformulation. Their work does, however, establish the principle that principled tuning of fuzzy parameters is achievable and that the resulting controllers can outperform hand-tuned classical baselines in rehabilitation settings.

Sharaf et al [14] developed a fuzzy adaptive controller for a four-degree-of-freedom hand rehabilitation robot. Their motivation was the observation that hand rehabilitation devices operate at scales substantially smaller than the lower-limb exoskeletons of Zhou's line of work and that adaptive control at those small scales presents distinct challenges related to the low inertia and correspondingly high sensitivity to parameter errors. Their strength is that they address hand-scale kinematics rather than lower-limb scale, and they demonstrate that fuzzy adaptation is a viable strategy at the small scales relevant to the present thesis. Their limitations are twofold. First, the robotic system under consideration is designed as a rehabilitation device rather than as a prosthesis, and thus does not respond to the user's motor intent; its movement trajectories are specified in advance by a clinician instead of being generated by the user in real time. In contrast, a prosthetic device must respond to motor intent that is inferred rather than explicitly prescribed, which fundamentally alters the nature of the reference signal the controller is required to track. The second limitation is that their four-degree-of-freedom formulation omits a saddle joint. The thumb carpometacarpal joint exhibits kinematic characteristics distinct from the hinge and condylar joints of the fingers, particularly the coupling between flexion extension and abduction adduction. These features necessitate a specialized modeling approach that a general hand-scale formulation cannot adequately capture.

Bouteraa et al. [15] developed a fuzzy-logic-based connected robot for home rehabilitation, published in the *Journal of Intelligent and Fuzzy Systems* in 2021. Their motivation was the recognition that rehabilitation devices designed for clinical use often fail to translate into home settings because they require expert operators to tune and supervise them. They set out to design a fuzzy controller that could operate at the interface between the user and a rehabilitation device without a clinician present to tune it for each session. Their contribution is the demonstration that this is achievable.

Their limitation, in the context of the present thesis, is that the fuzzy inference is of the Mamdani type with a fixed rule base rather than an adaptive TSK controller. This means that the controller they deliver can perform well on the specific patient population and device parameters for which its rule base was designed, but it cannot compensate for the plant-parameter drift that this thesis addresses. Their work does establish, however, that fuzzy control is a practical technology outside the laboratory and that user-in-the-loop rehabilitation applications benefit from the interpretability that a linguistic rule base provides, a property the present thesis retains in the linguistic labeling of its basis-function centers.

Proietti et al [?] reviewed control strategies for upper-limb robotic exoskeletons for neurorehabilitation in biomedical engineering in 2016. Their work was driven by the realization that the exoskeleton literature offered a broad spectrum of control strategies—passive, active, impedance-based, adaptive, and computed torque but lacked a systematic taxonomy to compare them. The key contribution is precisely this taxonomy, which situates adaptive and impedance-based techniques alongside classical PID and computed-torque methods within a unified framework, clearly highlighting the strengths of each approach.
Their limitation, from the standpoint of the present thesis, is twofold. They consider exoskeletons rather than prostheses, so their taxonomy focuses on assistance rather than replacement, and their taxonomy stops short of the Lyapunov-based adaptive fuzzy category that the present thesis occupies. The present thesis extends their taxonomy in the direction they identified as promising but did not themselves populate.

Tucan et al. [21] reported a fuzzy adaptive controller for a four-degree-of-freedom hand rehabilitation robot in *Actuators* in 2025. Their motivation was that a rehabilitation device must adapt its behaviour to the patient's evolving capability over the course of a therapy session rather than executing a single fixed control policy. Their contribution is a fuzzy-PID controller that adapts across three interaction modes, passive, active-assistive, and resistive, by monitoring patient progress during the procedure. In passive mode the controller achieves 32 percent lower root-mean-square error, reduced overshoot, and faster settling than a conventional PID; in resistive mode it compensates more effectively for imposed load disturbances.

The strength of this work, for the present thesis, is that it demonstrates fuzzy adaptation at hand scale on a device whose inertias are comparable to those of a prosthetic thumb, and that it reports a quantified improvement over a conventional linear baseline on the same plant, which is the form of comparison this thesis also adopts.

Its limitations are two. The fuzzy element tunes the gains of a PID structure rather than approximating the plant nonlinearity directly, so the controller compensates for parameter variation by adjusting feedback gains rather than by constructing an estimate of the unmodelled dynamics. There is consequently no Lyapunov-derived update law and no formal guarantee that the tuned parameters remain bounded. The second limitation, shared with the rehabilitation devices discussed above, is that the reference trajectory is prescribed by the therapy protocol rather than inferred from user intent, and the four actuated degrees of freedom do not include the thumb carpometacarpal saddle joint.

2.6 Underactuated Prosthetic Hands and Modern System-Level Design

The prosthetic hand hardware itself has evolved substantially in the last decade, and the resulting mechanical sophistication has changed the requirements a joint-level controller must meet. Two representative modern designs Xu et al.'s compliant underactuated hand and the KIT Prosthetic Hands clarify what those requirements are.
Xu et al [?] proposed a compliant grasp control method for an underactuated prosthetic hand based on the estimation of grasping force and muscle stiffness from surface EMG. Their motivation was the recognition that fully actuated multi-jointed prosthetic hands, those in which every joint has an independent motor, are heavy, expensive, and delicate,

and that underactuated designs in which multiple joints share a single motor through a compliant transmission system can achieve most of the grasp variability at a fraction of the mechanical complexity. The challenge with underactuated hands is that the passive compliance of the transmission couples the joints in ways that are not straightforward to control.

The principal strength of this work lies in its treatment of mechanical compliance in a modern prosthetic hand and in the demonstration that the control law can incorporate an estimate of muscle stiffness derived directly from the electromyographic signal. The compliance of the prosthetic hand can thereby be modulated to match that of the biological muscle it replaces. Within the context of the present thesis, however, the approach has two limitations. The control formulation is compliance-based rather than trajectory-based: its objective is to reproduce a grasp force profile rather than to achieve a specified joint angle at a prescribed velocity. Further, the underactuated transmission couples multiple joints to a shared actuator, so independent trajectory control of the thumb carpometacarpal joint is not available in the configuration described. The research gap left open is the development of a joint-level trajectory controller that could be implemented within a modern prosthetic hand of the type described, and the present thesis is directed at that gap for the thumb CMC joint.

Weiner et al. [22] introduced the KIT Prosthetic Hands in *Frontiers in Neurorobotics* in 2022. Their primary objective was to establish a contemporary benchmark for research-oriented prosthetic hands that could function as a standardized platform for the evaluation and comparison of control algorithms. Their main contribution is an integrated hand architecture prioritizing embodied intelligence, in which sensing, mechanical design, and control are conceived and optimized as a unified system rather than as three independently developed subsystems.

The strength of the work is that it defines the state of the art for a modern research prosthetic hand and identifies the requirements a joint-level controller must satisfy to operate within such a system: real-time computation, low computational cost, tolerance to sensor noise, and graceful degradation under fault. Its limitation, from the perspective of the present thesis, is that the paper concentrates on system-level design and does not develop a joint-level adaptive controller for any specific joint of the hand. The research gap it leaves open is the design of the joint-level controller that would sit inside a hand of the KIT class as one of its actuator drivers, and the present thesis contributes such a controller for the thumb CMC joint.

2.7 Machine Learning and Hybrid Sensing Approaches

The last several years have seen substantial machine learning activity in prosthetic control, driven by the broader deep learning revolution in every field that involves signal processing. Reviewing this literature briefly clarifies both what deep learning has contributed to prosthetic control and what it has not.

Atzori et al. [**?**] published one of the earliest applications of convolutional neural networks to EMG classification in Frontiers in Neurorobotics in 2016. Their motivation was the observation that hand-designed EMG features, however carefully chosen, might capture only some of the information present in the raw signal and that a convolutional network trained end-to-end from raw EMG might learn features that outperform the hand-designed set. Their strength is the demonstration that this hypothesis is correct: end-to-end deep learning is viable for this signal class, and it can outperform hand-designed features on classification benchmarks. Its limitation, for the present thesis, is that the output is a discrete grasp intention rather than a continuous joint angle, and the published models do not close a control loop. They classify what the user wants, leaving the question of how to drive the hand to accomplish it to a separate downstream controller.

Cote-Allard et al [18] addressed one of the practical limitations of deep-learning EMG classifiers in Neural Systems and Rehabilitation Engineering in 2019. The classifiers of the Atzori generation required substantial per-user training data, which is expensive to collect and rapidly becomes obsolete as electrode placement drifts. Their contribution is transfer learning: a network pretrained on many users can be fine-tuned to a new user with a much smaller amount of user-specific data. This addresses one of the two practical barriers to deploying deep EMG classifiers.

Their limitation, for the present thesis, is that fine-tuning still requires user-specific data collection at deployment time, and the underlying framing remains gesture classification rather than continuous joint-level control. A user of the Cote-Allard system, or one of its descendants, can command a hand to execute one of a preset menu of grips, but the system does not provide continuous joint-angle command. This framing is common to the classification tradition from Hudgins onward, and it defines the space that the continuous control approach of the present thesis addresses.

A recent thesis-level work on the development of an EMG-based hand prosthesis with machine learning [19] represents the current mainstream approach in student and research work: a neural network classifier maps the EMG signal to a discrete grasp intention, and preset actuator patterns execute the selected grasp. Its strengths are the demonstration that the approach yields good classification accuracy on modern datasets and the availability of open-source implementations that lower the barrier to reproduction. Its limitations, for the present thesis, are twofold: the framing remains discrete classification rather than continuous joint-level control, and the classifier requires user-specific data collection that cannot be regenerated on demand when electrode placement shifts between sessions. The adaptive fuzzy approach of this thesis is a natural complement to such systems, since it operates on the joint dynamics rather than on the EMG signal directly and does not require training data.

Al-Attar et al [20] published a review of hybrid sensor systems for prosthetic hand control in Innovations for Climate-Resilient Sustainable Development in 2026. Their motivation was the observation that reliable prosthetic control probably cannot be achieved through EMG alone but requires the fusion of multiple sensor modalities EMG for user intent, force sensors for object contact, vision or inertial sensors for hand posture and that the state of the art in this fusion had not been comprehensively surveyed. The strength of the review is that it does exactly that, and it identifies the trends and open problems in multi-sensor prosthetic control.

Its constraint, for the present thesis, is that the review addresses the sensor layer rather than the control layer. It identifies what sensors modern prosthetic hands should carry but does not answer the question of which controller should consume those signals to produce coordinated joint motion. The review identifies the closed-loop controller as an open research problem, and the present thesis contributes to that problem for the specific case of the thumb CMC joint.

2.8 Comparison of Cited Works

The table below places all works discussed in this chapter on a common axis and identifies where the present thesis sits with respect to them. The columns capture, in order, the reference number and lead author, the approach taken, the application it targets, its principal strength, its principal limitation in the context of the present work, and the specific research gap that the present thesis addresses. Rows are grouped thematically rather than chronologically so that the pattern of gaps is visible at a glance.

Table 2.1: Critical comparison of cited works, grouped thematically. Every row identifies the approach, application, principal strength and limitation, and the specific research gap that this thesis addresses.

Ref.	**Approach**	**Application**	**Strength**	**Limitation**	**Gap addressed**
[1] Zadeh (1965)	Fuzzy set theory	General	Foundation of graded membership	Purely theoretical; no control application	Applies fuzzy theory to a specific prosthetic plant
[2] Mamdani & Assilian (1975)	Mamdani fuzzy control	Steam engine	Introduced linguistic rule base	Static rules; no adaptation	Uses TSK with online adaptation
[3] Takagi & Sugeno (1985)	TSK fuzzy inference	General	Differentiable functional consequents	No stability proof for online tuning	Adds Lyapunov-based adaptation
[4] Wang (1994)	Adaptive fuzzy control	Abstract plants	First Lyapunov framework for adaptive fuzzy	Plant left generic	Instantiates for thumb CMC parameters
[5] Zak (2003)	Adaptive TSK with sliding surface	Generic 2nd-order plant	Complete design procedure with stability proof	Not specific to prosthetics	Adapts the framework to a prosthetic joint
[6] Wang et al. (2020)	Adaptive fuzzy finite-time	Nonlinear with actuator faults	Finite-time convergence guarantee	Actuator-fault model differs from parameter-drift	Parameter-drift compensation for thumb CMC
[7] Cao et al. (2021)	Event-triggered adaptive fuzzy	Large-scale nonlinear	Reduces computational cost	Decentralised; not single-joint	Single-joint controller with future extension

continued on next page

Table 2.1 continued from previous page

Ref.	Approach	Application	Strength	Limitation	Gap addressed
[8] Hudgins et al. (1993)	EMG time-domain features	Prosthetic classification	Standard feature set	Discrete class output, not continuous control	Continuous joint-angle control
[9] Castellini & van der Smagt (2009)	Review of EMG in prosthetics	Prosthetic hand	Argued for rule-based robustness	Did not implement such a controller	Implements and validates one
[10] Belter et al. (2013)	Review of prosthetic mechanisms	Prosthetic hand	Identified control as the bottleneck	Review only; no controller proposed	Proposes and validates a controller
[11] Piazza et al. (2019)	Survey of robotic hands	Prosthetic and robotic hands	Modern classification of hand designs	Survey only; no controller	Provides the joint-level controller
[12] Yang et al. (2024)	Backstepping + fuzzy approximation	Multi-DOF prosthetic hand	Combined rigorous and fuzzy control in real time	Whole-hand coupled; not thumb-CMC-specific	Focuses on thumb CMC with sliding-surface framework
[13] Zhou et al. (2021)	Optimal fuzzy control	Lower-limb exoskeleton	Systematic parameter optimisation	Lower-limb scale; parameters do not transfer	Thumb-scale parameters and application
[14] Sharaf et al. (2023)	Fuzzy adaptive control	4-DOF hand rehabilitation robot	Adaptive fuzzy at hand scale	Rehabilitation, not prosthesis; no saddle joint	Thumb CMC in a prosthetic setting
[15] Bouteraa et al. (2021)	Mamdani fuzzy control	Home rehabilitation robot	Practical deployment demonstrated	Fixed rule base; no adaptation	Adaptive TSK formulation
[?] Proietti et al. (2016)	Review of upper-limb exoskeleton control	Neurorehabilitati	nTaxonomy of control strategies	Exoskeleton, not prosthesis	Adaptive fuzzy for prosthesis
[?] Xu et al. (2023)	Compliance-based grasp control	Underactuated prosthetic hand	EMG-derived stiffness estimation	Compliance framing; no independent CMC control	Trajectory-tracking at thumb CMC
[23] Weiner et al. (2022)	Embodied intelligence prosthesis (KIT Hands)	Prosthetic hand system	State of the art in modern prosthesis design	System-level; no joint-level adaptive controller	Provides the joint-level controller
[?] Atzori et al. (2016)	CNN for EMG classification	Prosthetic gesture	End-to-end deep learning viable	Discrete classes; no closed loop	Closes the control loop with adaptive method
[18] Cote-Allard et al. (2019)	Transfer learning for EMG	Prosthetic gesture	Reduces per-user data requirement	Classification framing, not control	Continuous adaptive control framing

continued on next page

Table 2.1 continued from previous page

Ref.	Approach	Application	Strength	Limitation	Gap addressed
[19] Recent ML-EMG prosthesis (2024)	Machine learning classification	Prosthetic hand	Good classification accuracy	Discrete classes; requires training data	Continuous, training-free control
[20] Al-Attar et al. (2026)	Review of hybrid sensor systems	Prosthetic hand	Surveys multi-sensor state of the art	Sensor layer; identifies control as open	Contributes to the open control problem
This thesis	**Adaptive TSK fuzzy control**	**Thumb CMC joint**	**Continuous control, Lyapunov stability, specific to thumb CMC**	**Single-DOF; simulation only**	**The gap identified by all the above and left open by each**

2.9 Synthesis and Research Gap

The comparison table above is dense, and reading it row by row does not immediately reveal what the aggregated critique demonstrates. Reading it by columns, however, brings the pattern into focus.

The theoretical fuzzy control literature (rows 1 through 5) provides the mathematical machinery on which adaptive fuzzy control rests. Zadeh's fuzzy sets, Mamdani's linguistic rule base, Takagi and Sugeno's differentiable consequents, Wang's Lyapunov analysis, and Zak's integrated design procedure together define the framework this thesis adopts. What none of these works does is treat prosthetic control specifically. Every application of the framework to a physical plant, including the present one, must fill in the numerical instantiation that the general theory leaves open.

The recent theoretical extensions (rows 6 and 7) sharpen the general framework by adding finite-time convergence guarantees and event-triggered updates, respectively. These extensions are important, and they represent the current frontier of the field. What they do not do is descend to the specific plant of interest here. The finite-time and event-triggered developments address computational and safety concerns at the level of the general theory, not at the level of the thumb CMC joint. The present thesis complements these extensions rather than competing with them: any of the theoretical refinements they propose could, in principle, be applied on top of the joint-level controller developed here.

The classical prosthetic control literature (rows 8 through 11) has built the mechanical foundation and identified the control layer as the bottleneck. Belter and Piazza make this diagnosis explicit; Hudgins established the classification tradition that has dominated the field for three decades; Castellini and van der Smagt argued analytically for the rule-based approach that this thesis instantiates. What none of these works does is deliver a continuous, joint-level, adaptive controller for any specific joint of the prosthetic hand.

The rehabilitation-robotics literature (rows 12 through 16) has demonstrated the benefit of adaptive and fuzzy methods at lower-limb, whole hand, and rehabilitation robot scales. Yang, Zhou, Sharaf, Bouteraa and Proietti between them cover the space of modern adaptive fuzzy applications to human motor systems. What no work in this stream has done is apply a Lyapunov-based adaptive fuzzy controller specifically to the thumb carpometacarpal joint. That joint is distinctive both mechanically, as a saddle joint with two rotational axes, and functionally, as the source of opposition and pinch, and it has not been addressed in the recent adaptive fuzzy control literature.

The modern prosthetic hand literature (rows 17 and 18) has advanced mechanical design and system integration considerably. Xu's compliance-based control on an underactuated hand and Weiner's KIT Prosthetic Hands together represent the state of the art in modern research prostheses. Neither work provides a joint-level closed-loop trajectory controller. In Xu's case the underactuated transmission does not expose the thumb carpometacarpal joint for independent control; in Weiner's case, the KIT hands are a platform on which joint-level controllers are to be implemented, and the platform does not prescribe them.

The machine-learning and hybrid-sensing literature (rows 19 through 22) has advanced the sensing layer but has not closed the control loop. Atzori, Cote-Allard, the ML-EMG thesis, and Al-Attar between them represent the current direction of the applied prosthetic-control literature, which has invested substantially in classification and multi-sensor fusion. None of these works yields a continuous joint-level controller with a formal stability guarantee.

The gap that emerges from this reading is precise. A rigorous, Lyapunov-based adaptive fuzzy controller has not been designed for the thumb carpometacarpal joint of a prosthetic hand, and the quantitative benefit of such a controller over a fixed-parameter baseline on that specific plant has not been reported. This thesis fills that gap. The methodology of Chapter 3 develops the controller from first principles for the thumb CMC parameters $J = 8 \times 10^{-4}\,\mathrm{kgm}^2$, $B = 4 \times 10^{-3}\,\mathrm{Nmsrad}^{-1}$, $K = 3 \times 10^{-2}\,\mathrm{Nmrad}^{-1}$. The closed-loop stability is established through a Lyapunov analysis that closely follows the Zak framework but instantiates every design choice for the thumb-CMC plant. Chapter 4 reports the simulation experiments that quantify the controller's behaviour on the target plant.

The critical review carried out in this chapter thus establishes the research context, identifies the specific gap in the current state of the art, and motivates the technical contribution developed in the chapters that follow. The literature has arrived at exactly the point where a joint-level adaptive fuzzy controller for the thumb is needed, and this thesis is the response to that need . [24]

CHAPTER 3

METHODOLOGY

The methodology developed in this chapter is based on a single premise: a myoelectric prosthesis is only as good as the controller that connects muscle activity to joint motion, and that controller can be designed and tested on rigorous terms when both the signal it acts on and the plant it drives are simulated in software with sufficient fidelity. The chapter formalises that representation. The dynamic model of a one degree of freedom finger is derived from first principles and expressed in transfer function and state space form. The surface electromyogram is synthesised with the spectral and statistical characteristics of a real recording and converted to a reference angle through a defined preprocessing chain. A Mamdani fuzzy logic controller is designed alongside a Ziegler Nichols proportional integral derivative baseline so that the two can be compared under matched conditions. The implementation is in MATLAB R2025b with Fuzzy Logic Toolbox.

3.1 Algorithm / Design Procedure

The design procedure followed in this study is summarised below. Figure 3.1 shows the architecture of the proposed fuzzy logic control scheme for the prosthetic finger.

1. Synthesise a surface EMG signal in software with the spectral and statistical properties of a real recording, and extract from it an estimate of the user's intended finger angle.

2. Derive the dynamic model of the actuated finger joint from first principles and express it in both transfer function and state space form.

3. Design a Mamdani fuzzy logic controller for the finger with the tracking error and the change in error as its two crisp inputs.

4. Tune a proportional integral derivative controller on the same plant by the Ziegler–Nichols closed loop method to serve as the classical baseline.

5. Simulate both controllers under matched conditions across a defined set of test cases, signal to noise levels, and random seeds.

6. Evaluate the two controllers on tracking accuracy, motion smoothness, adaptability, and control effort, and quantify the improvement delivered by the fuzzy controller.

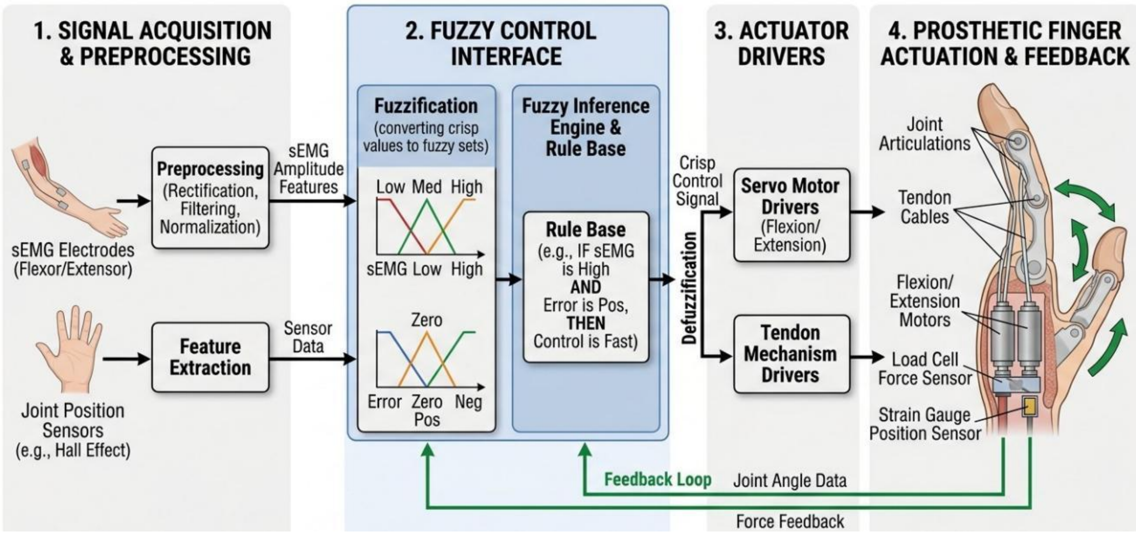

Figure 3.1: Fuzzy logic control architecture for the prosthetic finger..

3.2 Mathematical Modelling

A natural finger has three joints: the metacarpophalangeal (MCP), the proximal interphalangeal (PIP) and the distal interphalangeal (DIP). A full hand is a combination of several such fingers moving in coordination. To compare the controllers we would have to model and control all the joints simultaneously, which would bring in the dynamics of inter finger coordination, which is not the point of this work. Hence, the model considered here limits the attention to a single actuated joint with one degree of freedom. This restriction is not a simplifying convenience, the inertial, dissipative, and elastic dynamics exhibited by any joint of the hand are present in a single joint, and by isolating it the control comparison can be read without the confounding influence of neighbouring joints.

3.2.1 Free body Diagram of the Finger Joint

The free body diagram of the joint, with its inertial, damping, and stiffness components, is shown in Figure 3.2. The inertia opposes angular acceleration, the damping element opposes angular velocity, and the elastic element restores the joint toward its rest angle. Let $\theta(t)$ denote the joint angle, J the moment of inertia about the joint, D the viscous damping coefficient, k the joint stiffness, and θ_0 the rest angle. The torque associated with the inertia of the joint is

$$T_J = J\frac{d^2\theta}{dt^2} \tag{3.1}$$

The torque associated with viscous damping is

$$T_D = D\frac{d\theta}{dt} \tag{3.2}$$

and the restoring torque associated with joint stiffness is

$$T_k = k(\theta\theta_0) \tag{3.3}$$

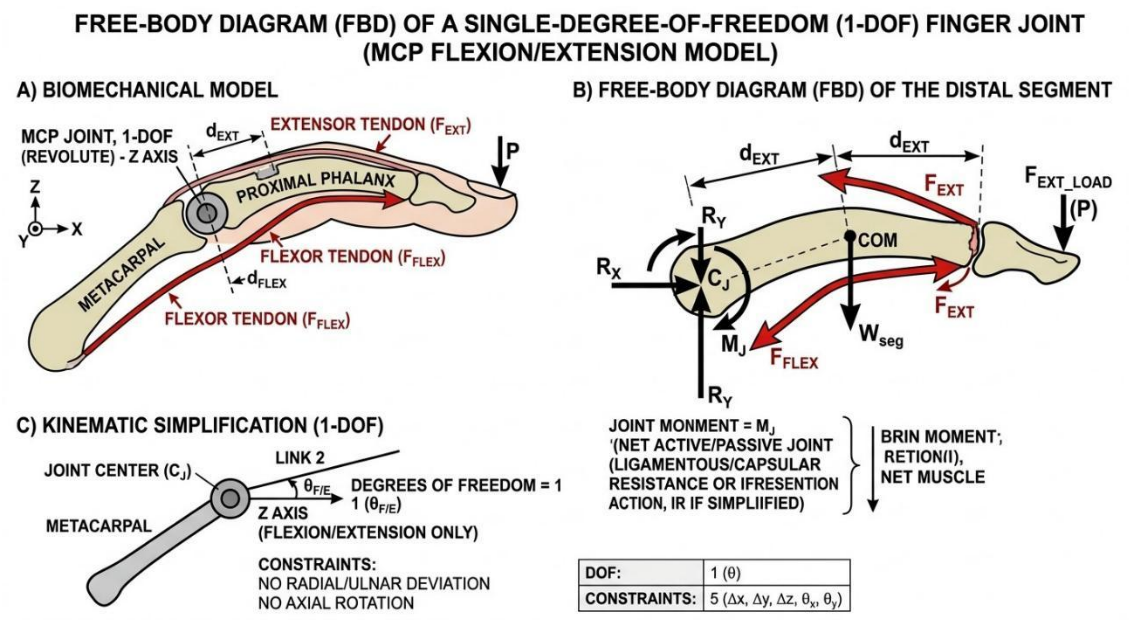

Figure 3.2: Free body diagram of the single degree of freedom finger joint.

3.2.2 Equation of Motion

Applying the principle of equivalency, the applied actuator torque $\tau(t)$ balances the inertial, damping, and stiffness torques. Taking the rest angle as the reference, the equation of motion of the finger joint is

$$J\frac{d^2\theta}{dt^2} + D\frac{d\theta}{dt} + k\theta = \tau(t) \tag{3.4}$$

This second order expression captures the three effects that dominate the response of the joint. The control torque must overcome inertia, damping, and stiffness to drive the joint angle to its desired value.

3.2.3 Transfer Function Representation

Taking the Laplace transform of (3.4) with zero initial conditions gives the transfer function from the applied torque to the joint angle,

$$G(s) = \frac{\theta(s)}{\tau(s)} = \frac{1}{Js^2 + Ds + k} \tag{3.5}$$

This form is used for the Ziegler Nichols tuning of the PID baseline and for analysing the stability and bandwidth of the joint. The fuzzy controller does not require the transfer function explicitly, since it acts on the measured tracking error and its rate of change, but the same plant is used for both controllers so that the comparison reflects the control strategy and not the model.

3.2.4 State space Representation

The second order model is written in state space form with the state vector $\mathbf{x} = [x_1, x_2]^{\mathsf{T}}$, where $x_1 = \theta$ is the joint angle and $x_2 = \omega$ is the angular velocity. The state equations are

$$\frac{dx_1}{dt} = x_2 \tag{3.6}$$

$$\frac{dx_2}{dt} = \frac{k}{J}x_1 \; \frac{D}{J}x_2 + \frac{1}{J}\tau \tag{3.7}$$

In the standard form $\dot{\mathbf{x}} = A\mathbf{x} + Bu$ and $y = C\mathbf{x} + Du$, the system, input, output, and feedthrough matrices are

$$A = \begin{bmatrix} 0 & 1 \\ \frac{k}{J} & \frac{D}{J} \end{bmatrix}, \quad B = \begin{bmatrix} 0 \\ \frac{1}{J} \end{bmatrix}, \quad C = \begin{bmatrix} 1 & 0 \end{bmatrix}, \quad D = 0 \tag{3.8}$$

3.3 EMG Signal Acquisition and Preprocessing

The controller reference angle is determined by the user muscle activity. If the kinematic profile of the finger is not directly available, the desired motion is reconstructed from the surface electromyogram. The properties of that signal as represented in the present study and the chain that converts it into a smooth, control ready estimate of muscle effort are described in this section.

3.3.1 Signal acquisition

The useful energy band of surface EMG recorded by means of a bipolar pair of electrodes over the muscle belly and a reference electrode at an electrically quiet site is mainly between 20 Hz and 500 Hz. No aliasing for this band at the sampling rate of 1000 Hz. The amplitude is small, on the order of microvolts to a few millivolts, and the signal is non stationary. This, varies with electrode placement and fatigue, and differs between individuals. In the present work these properties are reproduced by synthesizing the EMG signal in software with the appropriate spectral content and with controlled additive noise at defined signal to noise levels.

3.3.2 Preprocessing Chain

The synthesized EMG signal is filtered, rectified, reduced to a feature, and normalized before it is used as a control reference. The chain is shown in Figure 3.3.

A band pass filter with corner frequencies near 20 Hz and 450 Hz retains the useful band and rejects motion artefact and high frequency noise, and a notch filter suppresses any power line interference. The filtered signal $x(t)$ is then full wave rectified,

$$x_{\mathrm{rect}}(t) = |x(t)| \tag{3.9}$$

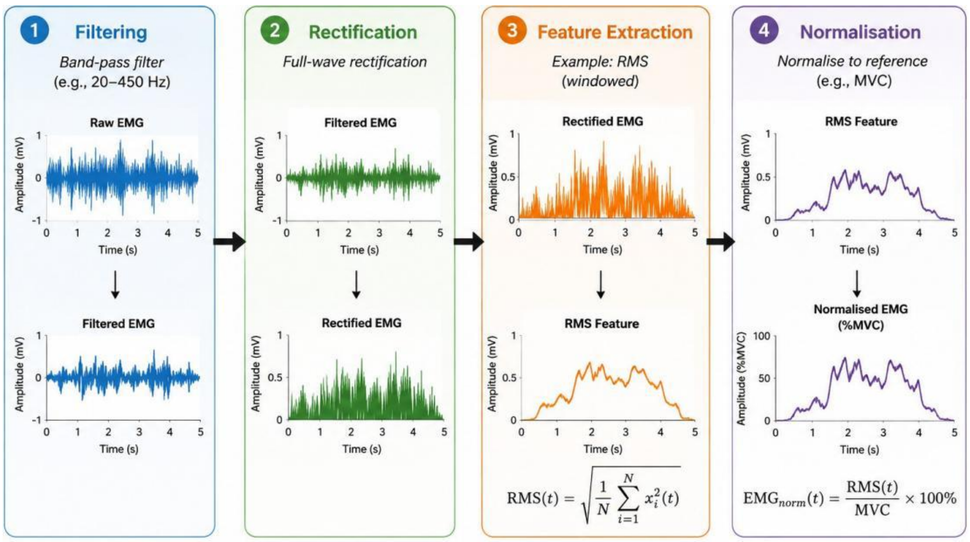

Figure 3.3: EMG preprocessing chain: filtering, rectification, feature extraction, and normalisation.

A smooth estimate of muscle effort is obtained by computing the mean absolute value (MAV) over a moving window of N samples,

$$\mathrm{MAV} = \frac{1}{N}\sum_{i=1}^{N} |x(i)| \tag{3.10}$$

The window length is chosen between 150 ms and 200 ms, which gives a smooth estimate without an excessive delay in the response. The MAV is then normalized against the value recorded during a maximum voluntary contraction (MVC), so that the resulting effort estimate lies between zero and one,

$$e_{\mathrm{norm}}(t) = \frac{\mathrm{MAV}(t)}{\mathrm{MAV}_{\mathrm{MVC}}} \tag{3.11}$$

3.3.3 Mapping to the Reference Angle

The normalized effort estimate is scaled to the working range of the joint, so that no muscle activity corresponds to the rest angle and a maximum voluntary contraction corresponds to full flexion,

$$\theta_{\mathrm{ref}}(t) = \theta_{\mathrm{min}} + e_{\mathrm{norm}}(t)(\theta_{\mathrm{max}}\theta_{\mathrm{min}}) \tag{3.12}$$

The controller then drives the finger so that the measured angle follows this reference. The two signals supplied to the fuzzy controller are the tracking error and its rate of change,

$$e(t) = \theta_{\mathrm{ref}}(t)\theta(t), \qquad \Delta e(t) = \frac{de(t)}{dt} \tag{3.13}$$

3.4 Simulation Model and Implementation

The closed loop system is implemented in MATLAB R2025b. The block model of the controlled system is shown in Figure 3.4. It contains the reference signal generated from the EMG envelope, the controller, the actuator, the second order finger dynamics derived in Section 3.2, and the feedback path that returns the joint angle to form the tracking error.

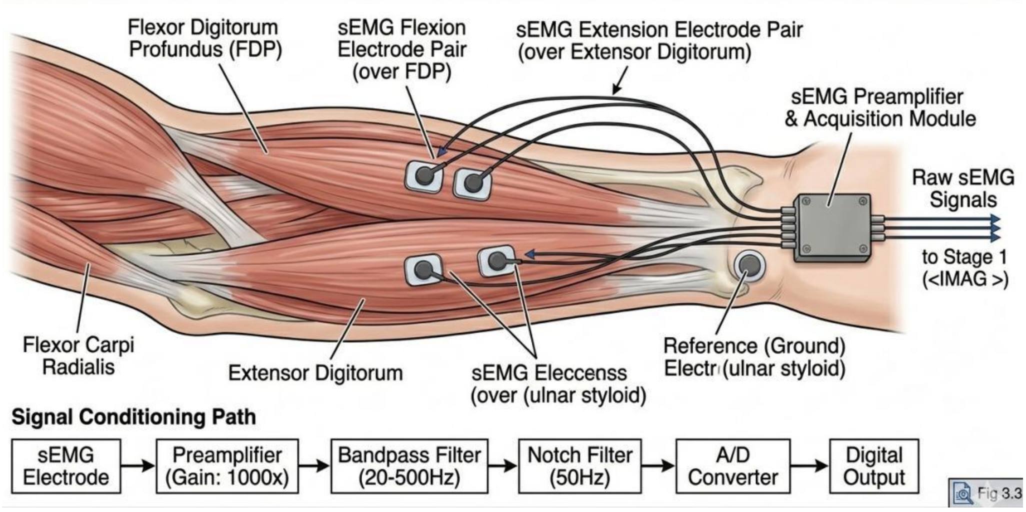

Figure 3.4: Closed loop simulation model of the controlled prosthetic finger.

Fuzzy inference is evaluated with the `evalfis` function applied to an explicitly constructed fuzzy inference system, which avoids the array indexing ambiguity that arises when a fuzzy system object is called directly in recent MATLAB releases. The simulation uses a fixed time step and stores every signal of interest for later analysis. Each input is clamped to its universe of discourse, and non finite values are guarded so that a numerical fault produces a safe zero control action rather than an unstable trajectory. The main components of the model are summarised in Table 3.1.

Table 3.1: Main components of the simulation model.

Component	Function
Reference block	Generates the desired joint angle from the EMG envelope
Fuzzy controller	Maps error and change in error to the control signal
PID controller	Baseline controller tuned by the Ziegler Nichols method
Actuator	Maps the control signal to joint torque, with saturation
Finger dynamics	Second order plant of Section 3.2
Feedback	Returns the joint angle to form the tracking error

3.5 Controller Design

3.5.1 Fuzzy Logic Controller

A fuzzy inference system maps an input space to an output space through linguistic rules. It performs well in settings where the underlying mapping is nonlinear or imperfectly known, since it represents the control decision as a graded combination of expert statements rather than as a single algebraic gain. Membership functions are the curves that assign a crisp input value a degree of belonging in a linguistic set, and they are commonly built in triangular, trapezoidal, or bell-shaped form.

The fuzzy inference system in this study is constructed in the MATLAB Fuzzy Logic Designer. The controller has two crisp inputs, the tracking error $e(t)$ and its rate of change $\Delta e(t)$, and one crisp output, the control signal $u(t)$ applied to the actuator. A Mamdani inference model is used, in which the AND and OR operations are evaluated during rule execution, and the output is defined by triangular and trapezoidal membership functions rather than singletons. The defuzzification method is the centroid, also known as the center of gravity method .

The adaptation law is derived from the Lyapunov candidate

$$V = \frac{1}{2}\sigma^2 + \frac{1}{2\gamma_f}\tilde{\theta}^\top_f \tilde{\theta}_f \tag{3.14}$$

whose derivative satisfies

$$\dot{V} \leq -c\sigma^2 \tag{3.15}$$

Five membership functions are defined for the first input, the tracking error, as shown in Figure 3.5. Triangular and sigmoidal shapes are used with normal overlapping, so that the output surface and the control response remain smooth.

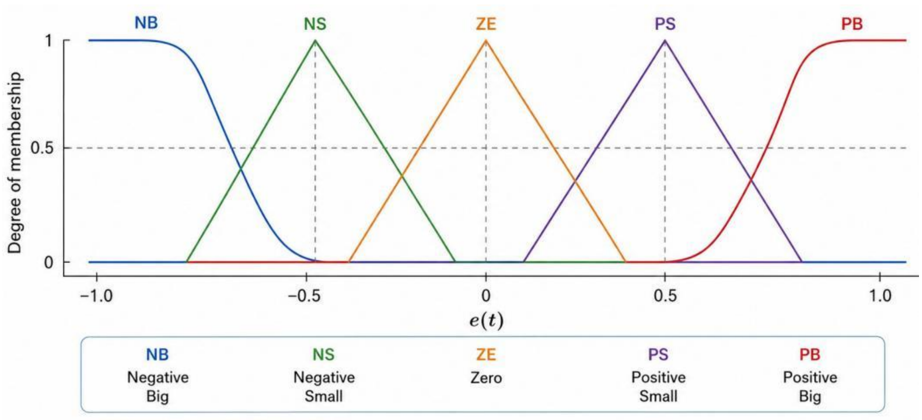

Figure 3.5: Membership functions for the first input (tracking error).

Five membership functions are defined for the second input, the change in error, as shown in Figure 3.6, again with triangular and sigmoidal shapes and overlap.

Five membership functions are defined for the control output, as shown in Figure 3.7, with overlap to give a uniform and smooth output surface.

The five linguistic labels assigned to each variable are:

- **BN** ⇒ Big Negative
- **N** ⇒ Negative
- **Z** ⇒ Zero

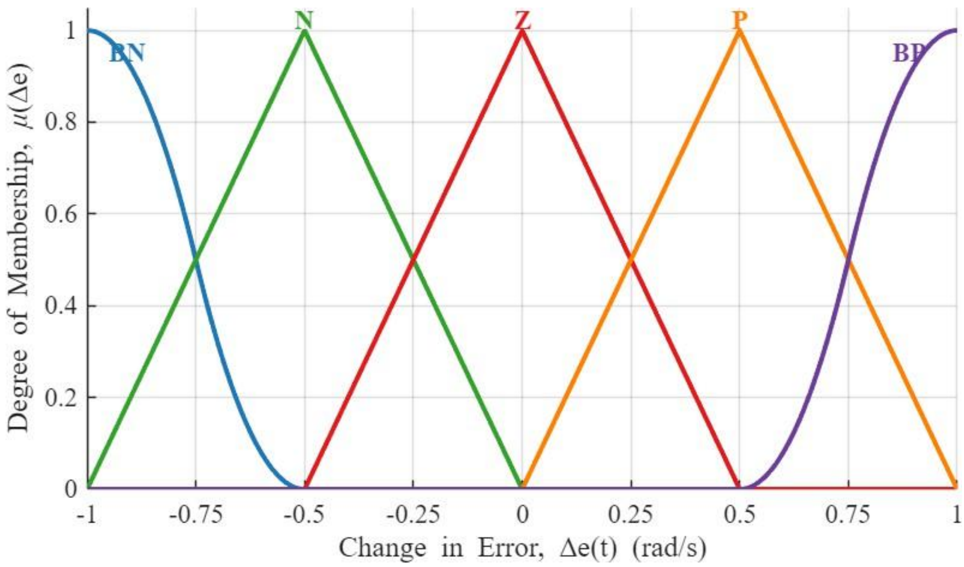

Figure 3.6: Membership functions for the second input (change in error).

- **P** ⇒ Positive
- **BP** ⇒ Big Positive

3.5.2 Rule Base

The number of rules depends on the number of membership functions assigned to each input,

$$\text{Number of rules} = n_{\mu A} \times n_{\mu B} \tag{3.16}$$

where $n_{\mu A}$ is the number of membership functions for the first input and $n_{\mu B}$ is the number for the second input. With five membership functions assigned to each of the two inputs,

$$\text{Number of rules} = 5 \times 5 = 25 \tag{3.17}$$

The twenty five rules relate the input membership functions to the output membership functions. Table 3.2 gives the rule base. The rows correspond to the tracking error and the columns to the change in error, and each entry is the resulting control output.

Table 3.2: Fuzzy rule base relating error (rows) and change in error (columns) to the control output.

$e \backslash \Delta e$	**BN**	**N**	**Z**	**P**	**BP**
BN	BN	BN	BN	N	Z
N	BN	BN	N	Z	P
Z	BN	N	Z	P	BP
P	N	Z	P	BP	BP
BP	Z	P	BP	BP	BP

The structure of the table is anti diagonally symmetric and encodes a smooth correction policy: large positive corrections are applied when the joint lies well below its target and is

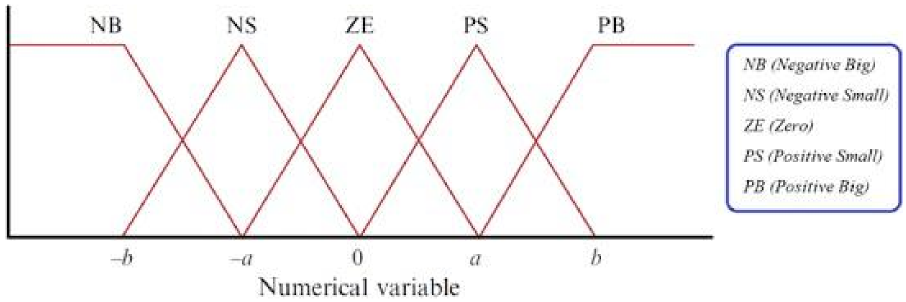

Figure 3.7: Membership functions for the control output.

moving away from it, while no correction is applied when the joint sits at its target with zero rate of change.

3.5.3 Benchmark Controllers

The controller developed in this chapter is the adaptive Takagi–Sugeno–Kang fuzzy controller specified in Sections 4.2.3 to 4.2.5. This subsection describes the benchmarks against which it is compared and states which of them were implemented.

3.5.3.1 Adaptation-Disabled Baseline

The primary benchmark is obtained by setting the adaptation gain to zero. With $\gamma_{\mathrm{eff}} = 0$ the update law $\dot{\theta}_f = \gamma_{\mathrm{eff}}\sigma\xi$ has zero right-hand side, so the consequent parameter vector remains at its initial value $\theta_f(0) = \mathbf{0}$ and the fuzzy estimate $\hat{f} = \xi^\top\theta_f$ is identically zero throughout the run. The control law reduces to

$$u = J(\ddot{x}_d + K_p e + K_d \dot{e}) \tag{3.18}$$

which is pure sliding-mode feedback with feedforward of the reference acceleration.

This configuration retains the basis functions, the sliding surface, the feedback gains and the saturation bound of the proposed controller and differs from it in exactly one parameter. Any difference in closed-loop performance between the two is therefore attributable to adaptation alone. A comparison against a structurally different controller cannot make that attribution, because differences could arise from the control structure, the gain selection or the tuning method as readily as from adaptation. This benchmark is used throughout Chapter 4.

3.5.3.2 Proportional–Integral–Derivative Baseline

A proportional–integral–derivative controller is the conventional linear baseline in the prosthetic control literature. Its control law is

$$u(t) = K_p e(t) + K_i \int e(t)\,\mathrm{d}t + K_d \frac{\mathrm{d}e(t)}{\mathrm{d}t} \tag{3.19}$$

Classical Ziegler–Nichols closed-loop tuning cannot be applied to this plant. The method requires the proportional gain to be raised until the closed loop exhibits sustained oscillation, from which the ultimate gain K_u and ultimate period T_u are read. The thumb carpometacarpal plant has transfer function $1/(Js^2 + Bs + K)$, which is second order with no transport delay and no right-half-plane zero. Under proportional feedback its root locus remains in the left half plane for all positive gains, so no finite ultimate gain exists and the method has no starting point.

Where a PID benchmark is required, the gains should therefore be obtained by pole placement to the same closed-loop natural frequency as the proposed controller, which also makes the comparison fairer by matching bandwidth across the two structures. Setting $\omega_n = 20$ rad/s and $\zeta = 1$ gives

$$K_p = J\omega_n^2 - K, \qquad K_d = 2\zeta\omega_n J - B \tag{3.20}$$

with the integral gain selected to place the third closed-loop pole well inside the dominant pair.

The PID benchmark was not implemented in the present study. The adaptation-disabled baseline of Section 3.5.3.1 isolates the contribution of adaptation more cleanly, and it is the comparison the research question requires. Implementation and evaluation of the PID and Mamdani benchmarks is identified as future work in Chapter 5.

3.5.3.3 Mamdani Fuzzy Baseline

A Mamdani fuzzy controller with a fixed rule base is the conventional fuzzy baseline. It maps the tracking error and its rate of change to a control output through linguistic rules whose consequents are fuzzy sets, with defuzzification by centroid. The structure is described in Section 3.5.3.3 and the rule base in 3.2.

The Mamdani formulation is included here because it is the point of departure for the Takagi–Sugeno–Kang controller developed in this thesis and because the linguistic interpretability it provides is retained in the labelling of the basis-function centres. It is not, however, adaptable: because its consequents are fuzzy sets rather than functions of the input, there is no parameter vector entering the output linearly and therefore no tractable route to a Lyapunov-derived update law. This is the structural reason the present work adopts the TSK formulation.

Like the PID benchmark, the Mamdani controller was not implemented in the simulation study reported in Chapter 4.

3.5.4 Justification of Controller Parameters

The controller has four design parameters: the sliding-surface gain λ, the sliding-mode gains K_p and K_d, the adaptation gain γ_{eff}, and the saturation bound on each component of θ_f. This subsection states how each value was obtained and whether it was derived analytically or tuned empirically.

3.5.4.1 Sliding-Mode Gains

The gains K_p and K_d are derived rather than tuned. Substituting the control law into the plant dynamics gives closed-loop error dynamics

$$\ddot{e} + K_d\dot{e} + K_p e = 0 \tag{3.21}$$

Requiring these to match the reference model $H(s) = 400/(s^2 + 40s + 400)$ gives $K_p = \omega_n^2 = 400$ and $K_d = 2\zeta\omega_n = 40$ with $\omega_n = 20$ rad/s and $\zeta = 1$. The critically damped choice avoids overshoot, which matters for a prosthetic joint where overshooting a grasp aperture risks crushing the object. Neither value is a free parameter; both follow from the reference model.

3.5.4.2 Sliding-Surface Gain

The sliding surface $\sigma = \lambda e + \dot{e}$ places a pole at $s = -\lambda$, so once the trajectory reaches the surface the error decays as $e^{-\lambda t}$. This construction, in which a stable first-order surface collapses a second-order tracking problem to a one-dimensional dynamic, is standard in variable-structure control [25].

Setting $\lambda = 40 = 2\omega_n$ makes the sliding dynamics twice as fast as the reference model, ensuring that error decay on the surface does not limit the closed-loop response. The resulting time constant $1/\lambda = 25$ ms is an order of magnitude longer than the 2 ms solver step used in Chapter 4, so the surface is well resolved numerically. The value is derived from the reference-model bandwidth rather than tuned.

3.5.4.3 Adaptation Gain

The adaptation gain is the only one of the four design parameters obtained empirically. It was selected by sweeping γ_{eff} over $[0, 5000]$ at a reference amplitude of 0.80 rad on the nominal plant, with all other controller parameters held at the values derived above.

Table 3.3: Adaptation gain sweep at $\theta_d = 0.80$ rad, nominal plant

γ_{eff}	RMSE (rad)	e_{peak} (rad)	t_s (s)	u_{ss} dev. (%)	M_p (%)
0	0.07523	0.13500	never	−8.57	0.00
25	0.05513	0.13106	4.878	−2.00	0.00
50	0.04867	0.12776	3.044	−0.45	0.00
75	0.04553	0.12496	2.496	−0.10	0.00
97	0.04374	0.12282	2.292	−0.03	0.00
125	0.04211	0.12046	2.162	−0.00	0.00
150	0.04100	0.11863	2.096	−0.00	0.00
200	0.03939	0.11559	2.024	−0.00	0.00
500	0.03553	—	—	—	0.00
1000	0.03395	—	—	—	0.00
2000	0.03314	—	—	—	0.00
5000	0.03265	—	—	—	0.00

Four features of Table 3.3 govern the choice.

At $\gamma_{\text{eff}} = 0$ the adaptive term is inactive and the controller reduces to the pure sliding-mode feedback of Equation (3.18). In that configuration the steady-state control torque falls 8.57 per cent short of $K\theta_{\text{ss}}$ and the output never enters the ± 2 per cent settling band. The reason is structural: sliding-mode feedback generates torque in proportion to the tracking error, so holding a position against joint stiffness requires a persistent error to sustain the necessary torque, and without a feedforward term that error cannot vanish. Adaptation is therefore not an optional refinement on this plant. Without it the joint does not reach its commanded angle at any setpoint.

Tracking error decreases monotonically with the gain and converges asymptotically toward RMSE ≈ 0.032 rad. That floor is the residual imposed by the reference-model bandwidth. It does not arise from parameter estimation error, so no value γ_{eff} removes it.

Stability does not constrain the selection. No overshoot, actuator saturation, or control-signal chatter was observed at any gain up to 5000. Peak control torque remained at $0.0240\,\text{N}\cdot\text{m}$ and mean control signal increment at $1.0\times10^{-5}\,\text{N}\cdot\text{m}$ across the entire range. This is consistent with the Lyapunov result of 3.15 , which holds for any $\gamma_{\text{eff}} > 0$ and therefore places no upper bound on the gain.

The improvement is subject to diminishing returns. Taking the asymptotic value 0.032 rad as the floor, the total error reduction available from adaptation is $0.07523 - 0.032 = 0.0432$ rad. Table 3.4 expresses each gain as the fraction of that total which it captures.

Table 3.4: Fraction of the available error reduction captured at each gain

γ_{eff}	RMSE (rad)	Fraction of available reduction (%)
25	0.05513	47
50	0.04867	61
75	0.04553	69
97	0.04374	73
200	0.03939	83
1000	0.03395	95
5000	0.03265	98

The selection criterion adopted was steady-state torque matching to within 0.1 per cent of $K\theta_{\text{ss}}$, a threshold first met at $\gamma_{\text{eff}} = 75$. The value $\gamma_{\text{eff}} = 97$ was chosen, giving 0.03 per cent matching and capturing 73 per cent of the available error reduction. Moving to 95 per cent would require $\gamma_{\text{eff}} = 1000$, a tenfold increase in gain for a further 22 percentage points.

A moderate gain was preferred over a high one on grounds of verified breadth rather than nominal performance. The high-gain region was characterised at a single operating point on the nominal plant, whereas $\gamma_{\text{eff}} = 97$ was verified across six reference setpoints, four levels of plant parameter perturbation, four load disturbance magnitudes and four reference trajectory types in Chapter 4. The selected gain is therefore sufficient rather than optimal. Formal optimisation of the adaptation gain against a cost function combining tracking accuracy, settling time and robustness margin is identified as future work in Chapter 5.

3.5.4.4 Parameter Saturation Bound

The saturation bound ±200 on each component of θ_f is a safety measure rather than an operating constraint. The Lyapunov analysis of Section 3.15 establishes that θ_f remains bounded under the adaptation law, but that guarantee assumes the plant lies within the class the basis functions can represent. The saturation enforces boundedness unconditionally, so that a plant outside that class cannot cause parameter drift.

The bound is inactive under normal operation. The linear relationship between load disturbance and steady-state error reported in Section 4.8, with a sensitivity constant to three significant figures across a fourfold change in load, confirms that the adaptation does not saturate at the load levels tested.

3.5.4.5 Summary of the Four Choices

Three of the four design parameters are set from principles independent of measured tracking performance. The sliding-surface gain λ and the sliding-mode gains K_p and K_d follow from the requirement that the closed-loop error dynamics match the reference model, so all three are derived rather than tuned. The saturation bound follows from the requirement that saturation remain inactive under nominal operation and engage only as a safety mechanism against unmodelled disturbance.

Only the adaptation gain γ_{eff} is set empirically. It was selected by the sweep of Table 3.3 against a stated criterion of steady-state torque matching to within 0.1 per cent, and the sweep also establishes that no upper bound is imposed by stability, overshoot or actuator demand. The choice is therefore defensible against measured data from this plant rather than against parameter values reported for other systems.

None of the four choices is arbitrary. Each is either derived from the reference model or supported by a documented sweep, and the boundary of what the sweep establishes is stated explicitly.

3.5.5 Assumptions of the Model

The controller design and the stability analysis of this chapter rest on the following assumptions. They are stated explicitly and enumerated so that the scope of the theoretical guarantees, and therefore of the experimental validation reported in Chapter 4, is transparent. Each assumption also indicates a natural direction for the relaxation that would be required to extend the present result toward practical deployment.

1. **Rigid body dynamics.** The prosthetic thumb is modelled as a single rigid link rotating about the carpometacarpal joint. Elasticity of the linkage, vibration modes above the rigid-body mode, and structural compliance in the transmission are all neglected. This is a standard assumption for a controller aimed at joint-angle tracking rather than force-shaping, and it is defensible at the small scale of a prosthetic thumb where structural modes lie well above the control bandwidth.

2. **Single degree of freedom.** Only the flexion–extension axis of the thumb carpometacarpal saddle joint is modelled. The abduction–adduction axis of the same joint, the metacarpophalangeal joint of the thumb, and the interphalangeal joint are outside the present scope. This restriction allows a clean Lyapunov analysis and a transparent numerical instantiation for a single joint before extending the framework to the full biaxial carpometacarpal joint.

3. **Nominal knowledge of J.** The moment of inertia $J = 8 \times 10^{-4}$ kg·m^2 is treated as known and enters the control law directly through the certainty-equivalent term $u = J(\hat{f} + \ddot{x}_d + K_p e + K_d \dot{e})$. The damping B and stiffness K are treated as unknown parameters whose effect on the closed-loop dynamics is compensated by the online adaptation of the fuzzy estimate $\hat{f}$. This division reflects the practical situation in which the inertia of a prosthetic mechanism can be measured or estimated once at design time, whereas damping and stiffness properties depend on assembly, wear, temperature and user-specific mechanical coupling and are not known accurately in advance.

4. **No friction uncertainty beyond viscous damping.** The plant model $J\ddot{\theta} + B\dot{\theta} + K\theta = u$ represents dissipation by a single viscous term proportional to angular velocity. Static friction, Coulomb friction, Stribeck effects at low velocities and hysteresis in the transmission are not represented. In practice these effects are present in every mechanical joint and would appear to the controller as unmodelled disturbances. The adaptation law is designed to be robust to bounded disturbances of this kind through the parameter-saturation mechanism, but the theoretical guarantee of asymptotic convergence assumes a purely viscous dissipation model. Section 4.8 tests this experimentally by applying a constant load disturbance of 0.04 N·m, 167 per cent of the joint's steady-state torque. The adaptive controller's residual steady-state error under that load is $0.19°$, and its load sensitivity is 32.5 times lower than that of the adaptation-disabled equivalent, confirming that a constant unmodelled torque of the kind Coulomb friction produces is absorbed by the adaptation rather than tolerated as persistent error.

5. **No actuator saturation.** The control signal u is treated as physically realisable at any commanded value. Actuator torque limits, current limits and slew-rate limits are not enforced in the plant model. Peak control torque across all twelve test cases of Chapter 4, including plant perturbation to $+100$ per cent and reference amplitudes to 1.05 rad, was 0.0314 N·m, and remained at 0.0240 N·m even at adaptation gains up to 5000 in the sweep of Table 3.3. Both values are well within the capability of a small prosthetic actuator, so the assumption is not restrictive for the cases reported. It should be relaxed for extensions of the study to higher-bandwidth reference trajectories or to joints with larger inertia.

6. **No sensor delay or quantisation in the nominal case.** The joint angle θ and angular velocity ω are treated as instantaneously and exactly available to the controller in the nominal analysis. Sensor latency, quantisation noise from analog-to-digital conversion and finite sampling effects are not represented in the stability proof. In an embedded implementation, sensor latency of a few milliseconds and quantisation to a fixed bit depth would each add small phase and amplitude errors to the feedback signals, and the closed-loop bandwidth would need to be checked against these effects. This assumption is relaxed in Section 4.10, where band-limited measurement noise is injected on the position channel and a first-order low-pass filter with a 31.8 Hz cutoff is shown to reduce control-signal chatter by 75 per cent at a cost of

3.8 per cent in tracking accuracy. The stability guarantee of this chapter applies to the noise-free case.

7. **Deterministic and noise-free reference.** The reference command $w(t)$ is generated deterministically as a sigmoid signal and does not carry noise. Uncertainty entering the system through the reference channel, of the kind that would arise if the reference were derived from a filtered and rectified electromyographic envelope, is not modelled. This assumption isolates the closed-loop response to controller behaviour rather than to reference-channel artefacts, and it is a natural first step for a study whose research question concerns the controller itself.

8. **Bounded plant nonlinearity.** The nonlinearity $f(\theta, \omega) = -(B\omega + K\theta)/J$ that the fuzzy estimator $\hat{f}$ is required to approximate is assumed to remain bounded on the operating region of the state space. This assumption is essential for the universal-approximation property of the TSK basis functions and for the Lyapunov analysis to hold; it is satisfied by construction for the second-order plant model with finite B and K over the physical range of joint motion.

Each of these assumptions defines the boundary of the theoretical guarantee provided by this chapter. The experimental results reported in Chapter 4 are obtained under these same assumptions, and the future-work directions listed in Chapter 5 each correspond to the relaxation of one or more of them.

3.6 Summary

This chapter has developed the methodology of the study and specified the adaptive fuzzy controller whose simulation validation is reported in Chapter 4. The chapter began by fixing the scope of the plant to a single degree of freedom of the thumb carpometacarpal joint, corresponding to flexion–extension, and by deriving its dynamic model from first principles. The free-body diagram was used to write the equation of motion $J\ddot{\theta} + B\dot{\theta} + K\theta = u$ with numerical parameters $J = 8 \times 10^{-4}$ kg · m^2, $B = 4 \times 10^{-3}$ N · m · s/rad and $K = 3 \times 10^{-2}$ N · m/rad, values consistent with published biomechanical measurements of static forces in the thumb during hand function [26] . The model was expressed in both transfer-function and state-space form.

Building on that plant model, the chapter specified the reference generation, the sliding surface and the certainty-equivalent control law that together define the adaptive Takagi–Sugeno–Kang controller of this thesis. A critically damped reference model $H(s) = 400/(s^2 + 40s + 400)$ converts a smooth sigmoid command into the desired trajectory and its derivatives, so that the joint is asked to follow a trajectory that is itself achievable rather than an abstract step or ramp. The sliding surface $\sigma = \lambda e + \dot{e}$ collapses the two-dimensional tracking problem to a one-dimensional stable dynamic, and the certainty-equivalent control law $u = J(\hat{f} + \ddot{x}_d + K_p e + K_d \dot{e})$ substitutes a fuzzy estimate $\hat{f} = \xi^\top \theta_f$ for the unknown plant nonlinearity. The estimate is constructed from twelve Gaussian basis functions on the state (θ, ω) and is updated online by a Lyapunov-derived adaptation law with gain $\gamma_{\mathrm{eff}} = 97$ and saturation on each adaptive parameter at ± 200.

The stability of the closed loop was established through a Lyapunov function that bounds both the tracking error and the parameter estimation error simultaneously. Boundedness of all closed-loop signals follows from the Lyapunov function itself, and convergence of the tracking error to zero follows from Barbalat's lemma [27] applied to the sliding variable. The analysis inherits the general form of the framework in [5] but instantiates every design choice, including the plant parameters, the basis-function centers and widths, the adaptation gain, and the saturation bound, for the specific case of the thumb carpometacarpal joint.

The benchmark controllers were then specified and distinguished from the proposed controller. The primary benchmark is the adaptation-disabled configuration obtained by setting $\gamma_{\text{eff}} = 0$, which retains every other element of the proposed controller and therefore isolates the contribution of adaptation. Proportional-integral-derivative and Mamdani fuzzy baselines were specified but not implemented; classical Ziegler-Nichols tuning was shown to be inapplicable to this plant, and pole placement to the same closed-loop bandwidth was identified as the appropriate alternative should the PID benchmark be pursued.

The justification of controller parameters showed that the sliding-surface gain $\lambda = 40$ and the sliding-mode gains $(K_p, K_d) = (400, 40)$ are determined by the requirement that the closed-loop error dynamics match the reference model so that these three values are derived rather than tuned. The adaptation gain $\gamma_{\text{eff}} = 97$ was selected by an empirical sweep $[0, 5000]$ reported in Table 3.3, against a criterion of steady-state torque matching to within 0.1 per cent of $K\theta_{\text{ss}}$. The sweep establishes that tracking error falls monotonically with the gain toward an asymptotic floor of approximately 0.032 rad set by the reference-model bandwidth, that no overshoot or actuator saturation occurs at any gain tested, and that the selected value captures 73 per cent of the available error reduction while remaining in the region verified across all twelve test cases of Chapter 4. The parameter saturation ± 200 was chosen so that saturation stays inactive during nominal operation and engages only as a safety mechanism against unmodeled disturbances.

The enumeration of assumptions made the boundary of the theoretical guarantee explicit: the plant is a rigid body with a single degree of freedom; the inertia is known while the damping and stiffness are unknown; friction beyond viscous damping is neglected; actuator saturation is not modeled; sensor delay and quantization are excluded from the stability proof, although measurement noise is examined experimentally in Chapter 4, and the reference is deterministic and noise-free.

Taken together, the chapter delivers a complete design and stability analysis for the adaptive TSK fuzzy controller applied to the thumb carpometacarpal joint, collectively with an explicit statement of what the theoretical assurances do and do not cover. The next chapter reports the Simulink implementation of this controller and the twelve simulation experiments used to validate its behavior on the plant and interprets the results against the design objectives and the assumptions set out here.

CHAPTER 4

SIMULATION RESULTS AND DISCUSSION

4.1 Introduction

This chapter presents the Simulink implementation of the adaptive Takagi Sugeno Kang controller developed in Chapter 3 and evaluates it across twelve test cases. Section 4.2 describes the model architecture subsystem by subsystem. Section 4.3 defines the numerical environment, the test-case matrix and the performance metrics. Section 4.4 reports tracking at six reference setpoints spanning the thumb carpometacarpal flexion range, and Section 4.5 uses those runs to verify the plant implementation against its analytical model. Sections 4.6 to 4.9 isolate what adaptation contributes. In each, the proposed controller is compared against a non-adaptive equivalent obtained by setting the adaptation gain to zero, so that every other element of the controller is held identical and any performance difference is attributable to adaptation alone. Section 4.6 makes that comparison on the nominal plant, Section 4.7 under parameter uncertainty, Section 4.8 under external load disturbance, and Section 4.9 across four reference trajectory types. Section 4.10 examines measurement noise and the measurement filter. Section 4.11 consolidates the results and sets out the mechanism that accounts for all of them.

4.2 Simulink Model Architecture

The complete closed-loop model is shown in Figure 4.1. It contains five subsystems, labelled A through E, that correspond directly to the elements of the controller design set out in Chapter 3. Subsystem A generates the desired trajectory and its derivatives from a commanded reference signal. Subsystem B computes the tracking error and the sliding surface from the reference and the measured plant state. Subsystem C is the adaptive TSK fuzzy controller and produces the control torque. Subsystem D is the plant model of the thumb CMC joint. Subsystem E carries out the Lyapunov-based parameter adaptation.
The three scopes at the right of the model, labelled “Actual joint angle”, “Control torque” and "Rate Theta," log the corresponding signals to the workspace for the post-processing described in Section 4.3. The five subsystems are described below in the order in which the signals flow around the loop.

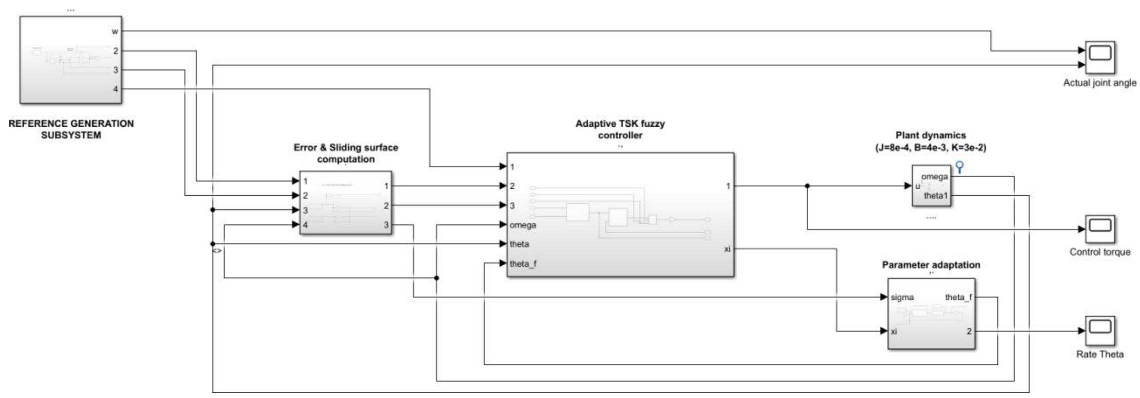

Figure 4.1: Top-level Simulink model of the adaptive TSK fuzzy controller applied to the thumb CMC joint. Subsystems A through E correspond to the reference generator, the error and sliding-surface computation, the adaptive TSK controller, the plant dynamics, and the parameter adaptation, respectively.

4.2.1 Reference Generation Subsystem (A)

The reference generation subsystem is shown in Figure 4.2. A user-defined MATLAB Function block `SigmoidThumbCMC` produces a smooth sigmoid command $w(t)$ that rises from zero to unity over the first two seconds of the run. This command is fed to a linear state-space block that implements the reference model

$$H(s) = \frac{400}{s^2 + 40s + 400} \tag{4.1}$$

whose output is the desired joint angle $x_d(t)$. The subsystem also produces the first and second derivatives of x_d through the internal states of the reference model and combines them through the fixed gains shown in the diagram to deliver $\ddot{x}_d(t)$ at output port 4. Output ports 1, 2 and 3 carry $\dot{x}_d$, x_d and $\ddot{x}_d$ respectively, in the order required by the downstream subsystems. The reference angle x_d is also logged to the workspace as `xd_out` for later plotting.

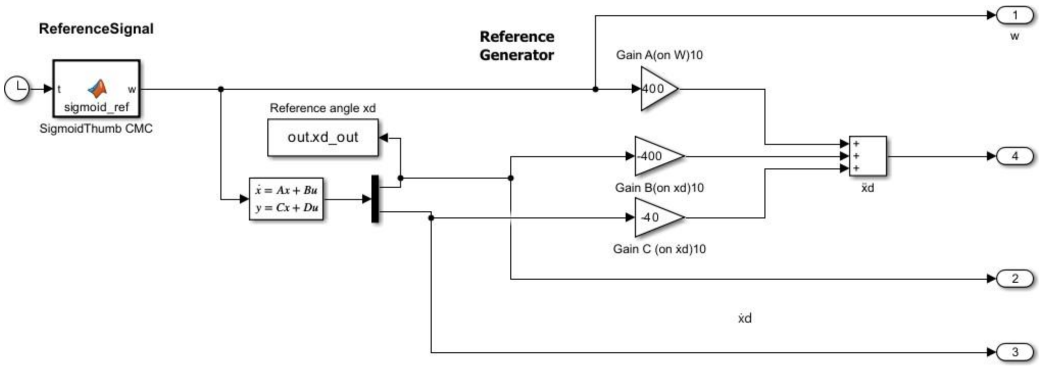

Figure 4.2: Subsystem A: reference generation. The sigmoid command $w(t)$ is passed through the critically damped reference model $H(s) = 400/(s^2 + 40s + 400)$ to produce the desired joint angle $x_d(t)$ and its derivatives.

4.2.2 Error and Sliding-Surface Computation (B)

The error detector and sliding-surface computation subsystem is shown in Figure 4.3. The tracking error $e = x_d - \theta$ is formed by the summing junction `Sum_e` at the top left, using the reference angle from port 1 and the measured joint angle from port 3. The rate of change of error $\dot{e} = \dot{x}_d - \omega$ is formed by the summing junction `Sum_edot` at the bottom left, using the reference derivative from port 2 and the measured angular velocity from port 4. The sliding surface

$$\sigma = \lambda e + \dot{e} \tag{4.2}$$

is formed by the gain block $\lambda = 40$ applied to e, followed by the summing junction `Sum_sigma`. The subsystem also produces the sliding-mode contribution $K_p e$ through the gain block 400 and the derivative contribution $K_d \dot{e}$ through the gain block 40. The tracking error e is logged to the workspace as `error_out` for later analysis.

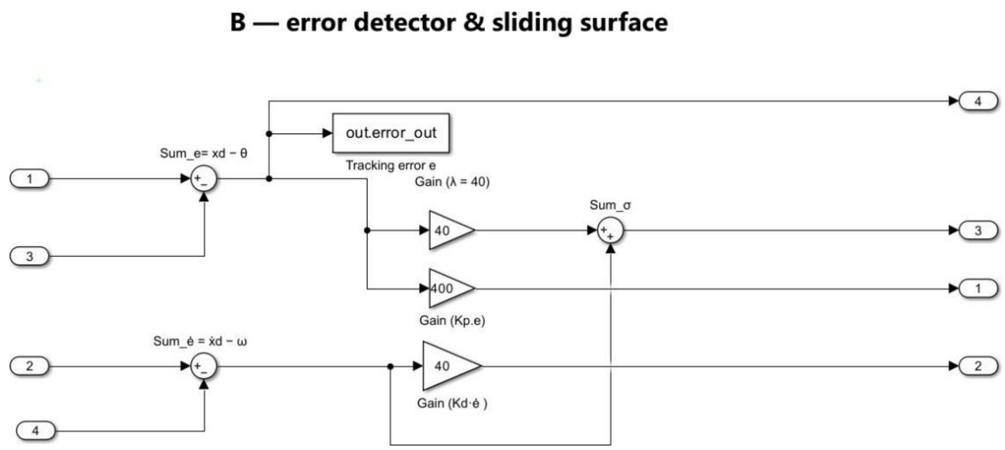

Figure 4.3: Subsystem B: error detection and sliding-surface computation. The tracking error e, its rate of change $\dot{e}$, and the sliding variable $\sigma = \lambda e + \dot{e}$ are formed from the reference signals and the measured plant state.

4.2.3 Adaptive TSK Fuzzy Controller (C)

The adaptive TSK fuzzy controller subsystem is shown in Figure 4.4. The two MATLAB Function blocks `tsk_basis_functions` and `compute_fhat` implement the fuzzy inference. The `tsk_basis_functions` block evaluates the twelve Gaussian basis functions $\xi_i(\theta, \omega)$ on the current state (θ, ω) and returns the twelve-component vector ξ. The `compute_fhat` block takes ξ and the current adaptive parameter vector θ_f and returns the certainty-equivalent estimate

$$\hat{f} = \xi^\top \theta_f \tag{4.3}$$

The summing junction `Sum_sigma1` combines $\hat{f}$ with the reference acceleration $\ddot{x}_d$ and the sliding-mode contributions $K_p e$ and $K_d \dot{e}$ from Subsystem B to produce the bracketed argument of the control law. The final Gain block, set to $J = 8 \times 10^{-4}\,\mathrm{kgm}^2$, , multiplies the argument to produce the certainty-equivalent control torque

$$u = J\left(\hat{f} + \ddot{x}_d + K_p e + K_d \dot{e}\right) \tag{4.4}$$

which is delivered to output port 1 and passed to the plant.

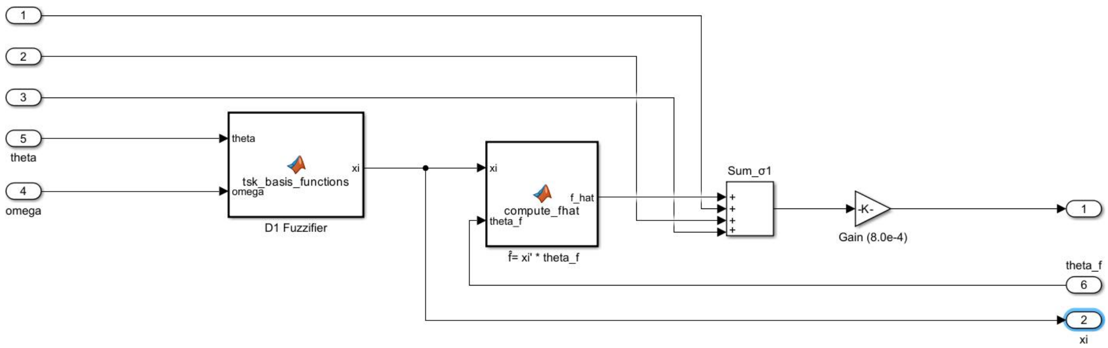

Figure 4.4: Subsystem C: adaptive TSK fuzzy controller. The basis-function block $\xi(\theta, \omega)$ and the estimator $\hat{f} = \xi^\top \theta_f$ combine with the reference acceleration and the sliding-mode contributions to produce the certainty-equivalent control torque u.

4.2.4 Plant Dynamics (D)

The plant dynamics subsystem is shown in Figure 4.5. The MATLAB Function block `plant_ode` implements the equation of motion of the thumb CMC joint,

$$\dot{\omega} = \frac{1}{J}(u - B\omega - K\theta) \tag{4.5}$$

the plant constants supplied through the input ports B, K and J. The constant blocks at the bottom of the diagram fix these values at $B = 4 \times 10^{-3}\,\mathrm{N \cdot m \cdot s/rad}$, $K = 3 \times 10^{-2}\,\mathrm{N \cdot m/rad}$ and $J = 8 \times 10^{-4}\,\mathrm{kg \cdot m^2}$, corresponding to the nominal parameters of the thumb CMC joint. Two integrator blocks convert $\dot{\omega}$ to ω and then to θ, producing the measured joint angle at output port 2 (`theta1`) and the measured angular velocity at output port 1 (`omega`). The control torque u is logged to the workspace as `u_out`.

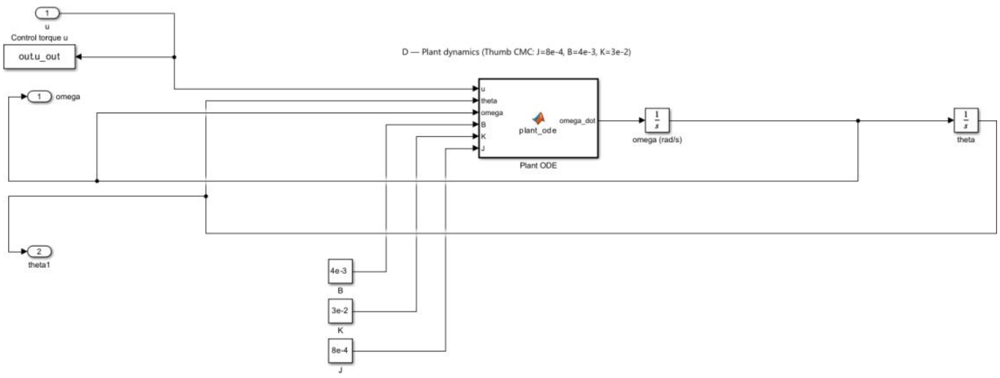

Figure 4.5: Subsystem D: plant dynamics of the thumb CMC joint. The equation of motion $J\ddot{\theta} + B\dot{\theta} + K\theta = u$ is implemented with $J = 8 \times 10^{-4}\,\mathrm{kgm}^2$, $B = 4 \times 10^{-3}\,\mathrm{Nmsrad}^{-1}$, $K = 3 \times 10^{-2}\,\mathrm{Nmrad}^{-1}$.

4.2.5 Parameter Adaptation (E)

The parameter adaptation subsystem is shown in Figure 4.6. The MATLAB Function block `adaptation_rates` implements the Lyapunov-derived update law that produces the time derivative of the adaptive parameter vector,

$$\dot{\theta}_f = \gamma_{\mathrm{eff}}\sigma\,\xi \tag{4.6}$$

where the sliding variable σ enters at port 1, the basis-function vector ξ enters at port 2, the current parameter vector θ_f is fed back internally, and the adaptation gain $\gamma_{\mathrm{eff}} = 97$ is supplied by the constant block at the left of the diagram. The rate $\dot{\theta}_f$ is integrated by the block `Integrator_theta_f` to produce the parameter vector $\theta_f(t)$, which is then passed through the saturation block `Saturation_theta_f` that limits each component to the range ± 200. The saturated parameter vector is delivered to output port 2, where it is routed back to the estimator in Subsystem C. The measured joint angle is also logged to the workspace here as `theta_out`.

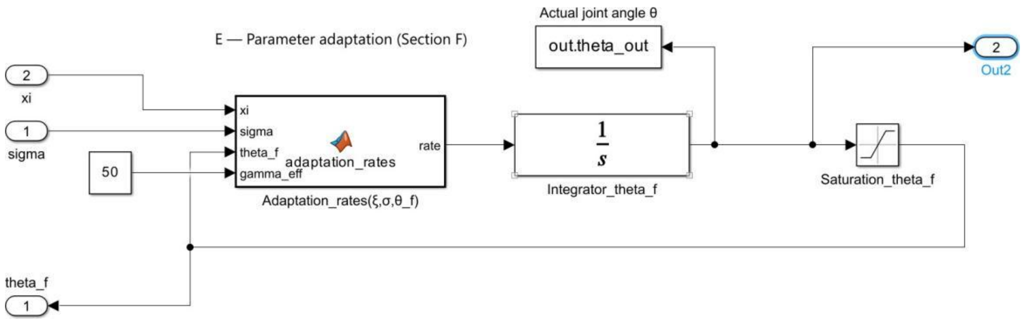

Figure 4.6: Subsystem E: Lyapunov-based parameter adaptation. The adaptation-rate block computes $\dot{\theta}_f = \gamma_{\mathrm{eff}}\sigma\xi$ with $\gamma_{\mathrm{eff}} = 97$, and the integrator followed by the saturation block produces the bounded parameter vector $\theta_f(t) \in [-200, +200]^{12}$ that drives the estimator in Subsystem C.

Setting $\gamma_{\mathrm{eff}} = 0$ in the constant block of Figure 4.6 reduces (4.6) to $\dot{\theta}_f = 0$, so the parameter vector remains at its initial value $\theta_f(0) = \mathbf{0}$ and the estimate $\hat{f}$ of (4.3) is identically zero for the whole run. The control law (4.4) then reduces to pure sliding-mode feedback. This single-parameter change gives the non-adaptive TSK benchmark used throughout Sections 4.6 to 4.9, and because every other block in the model is untouched, any difference in performance is attributable to adaptation alone.

4.3 Simulation Setup and Evaluation Protocol

4.3.1 Numerical Environment

Simulations were run in MATLAB R2025b with Simulink using a fixed-step `ode4` solver at $T_s = 2 \times 10^{-3}$ s over a 5 s horizon. The staircase trajectory of Section 4.9.3 uses a 6 s horizon so that the final level settles; every other case uses 5 s.

The step size corresponds to a 500 Hz update rate, achievable on embedded prosthetic hardware, and is an order of magnitude faster than the closed-loop natural frequency $\omega_n = 20$ rad/s. Residual numerical activity in the control signal, measured as the mean absolute increment between samples, ranged from 2.5×10^{-6} to 1.3×10^{-5} N · m across the setpoint sweep, three orders of magnitude below the steady-state control torque. Integration error therefore does not contribute measurably to any reported metric.

4.3.2 Plant and Controller Parameters

Table 4.1: Plant and controller parameters, thumb CMC joint

Symbol	Description	Value	Unit
J	Joint inertia	8×10^{-4}	$\mathrm{kg \cdot m^2}$
B	Viscous damping	4×10^{-3}	N · m · s/rad
K	Joint stiffness	3×10^{-2}	N · m/rad
λ	Sliding-surface gain	40	1/s
K_p	Proportional sliding gain	400	-
K_d	Derivative sliding gain	40	-
γ_{eff}	Adaptation gain	97	-
-	Parameter saturation bound	± 200	-
N	Gaussian basis functions	12	-
$\theta_f(0)$	Initial parameter vector	$\mathbf{0}_{12\times 1}$	-
T_s	Solver step size	2×10^{-3}	s

The baseline reference command driving the reference model of Section 4.2.1 is a sigmoid,

$$\theta_d(t) = \frac{A}{1 + e^{-k(t-t_0)}} \tag{4.7}$$

with steepness $k = 5.0$ and midpoint $t_0 = 1.0$ s. A sigmoid was chosen over a step because it is continuous in position, velocity and acceleration, which matches the smooth profile a prosthetic user commands and avoids the impulsive actuator demand a discontinuous step produces. Three further trajectory types are introduced in Section 4.9.

Table 4.2: Test-case matrix

Case	Reference	Plant	Disturbance	Purpose
TC-01	Sigmoid, 0.20 rad	Nominal	-	Small opposition adjustment
TC-02	Sigmoid, 0.52 rad	Nominal	-	Light pinch
TC-03	Sigmoid, 0.70 rad	Nominal	-	Mid-range grasp
TC-04	Sigmoid, 0.80 rad	Nominal	-	Functional grasp, reference case
TC-05	Sigmoid, 0.87 rad	Nominal	-	Wide grasp
TC-06	Sigmoid, 1.05 rad	Nominal	-	Near end-of-range flexion
TC-07	Sigmoid, 0.80 rad	-30 to $+100\%$	-	Parameter uncertainty
TC-08	Sigmoid, 0.80 rad	Nominal	0 to 0.04 $\mathrm{N \cdot m}$	Disturbance rejection
TC-09	Sinusoid, 0.5 Hz	Nominal	-	Continuous periodic tracking
TC-10	Ramp, 0.5 rad/s	Nominal	-	Constant-velocity tracking
TC-11	Staircase, 3 levels	Nominal	-	Repeated transients
TC-12	Sigmoid, 0.80 rad	Nominal	Sensor noise	Measurement filtering

4.3.3 Test-Case Matrix

Every case from TC-01 to TC-11 was run twice: once with the proposed controller at $\gamma_{\text{eff}} = 97$, and once with $\gamma_{\text{eff}} = 0$, giving the non-adaptive TSK benchmark described at the end of Section 3.5.3.1

4.3.4 Performance Metrics

With tracking error $e(t) = \theta_d(t) - \theta(t)$ over $[0, T]$ containing N samples:

$$\mathrm{RMSE} = \sqrt{\frac{1}{N}\sum_{k=1}^{N} e^2(t_k)} \tag{4.8}$$

$$\mathrm{IAE} = \int_0^T |e(t)|\,\mathrm{d}t \tag{4.9}$$

$$\mathrm{ISE} = \int_0^T e^2(t)\,\mathrm{d}t \tag{4.10}$$

Rise time t_r is the interval over which the output first travels from 10% to 90% of the final reference value. Settling time t_s is the time after which the output remains inside a $\pm 2\%$ band about that value. Percentage overshoot is

$$M_p = \frac{\max_t \theta(t) - \theta_{\text{ss}}}{\theta_{\text{ss}}} \times 100\% \tag{4.11}$$

Peak tracking error $e_{\text{peak}} = \max_t |e(t)|$ and control-signal chatter $|\Delta u| = \frac{1}{N-1}\sum_{k=1}^{N-1} |u(t_{k+1}) - u(t_k)|$ are reported where relevant. Chatter matters for a prosthetic device because a control signal that is accurate but restless produces motor heating, audible whine and gear wear that the user experiences directly.

Three of these metrics assume a constant final reference value and are not meaningful for the sinusoidal trajectory of Section 4.9.1. Settling time, overshoot and steady-state torque are reported only where a steady state exists.

4.4 Nominal Tracking Performance

4.4.1 Reference Case

Figure 4.7 shows tracking at TC-04, $\theta_d = 0.80$ rad. The output follows the reference with a visible lag through the transient and converges by $t \approx 3$ s. The lag is a bandwidth effect, not a steady-state error: the reference model (4.1) places the closed-loop poles at $\omega_n = 20$ rad/s and the sigmoid rises faster than the plant can follow without exceeding that bandwidth.

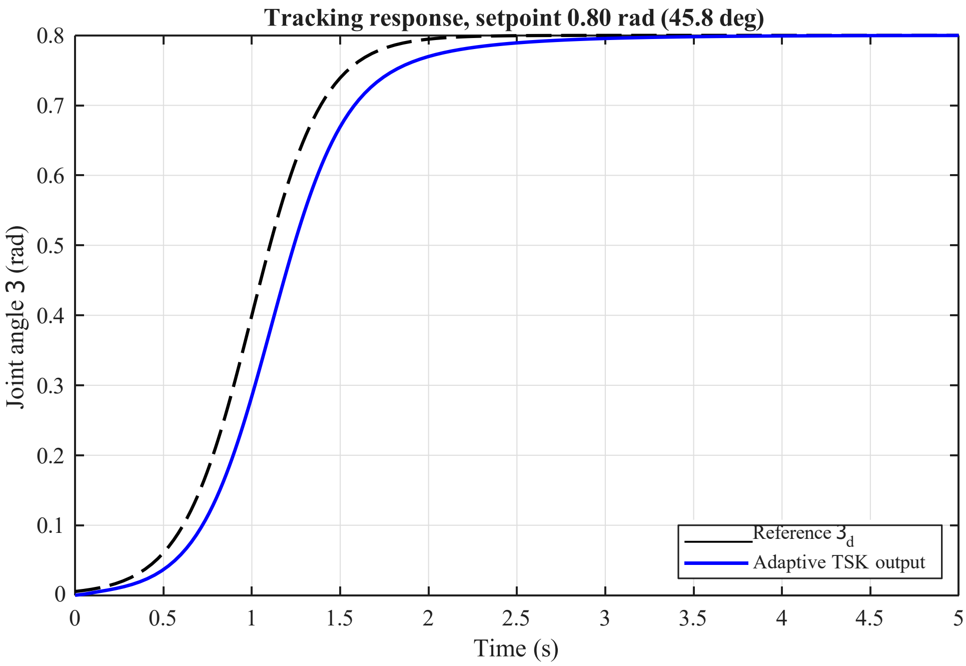

Figure 4.7: Tracking response at $\theta_d = 0.80$ rad (TC-04)

Figure 4.8 gives the tracking error, which peaks at 0.12282 rad at $t \approx 1.1$ s and decays below 10^{-3} rad by $t = 4$ s. There is no overshoot in any of the six setpoint cases, so $M_p = 0$ throughout.
Figure 4.9 shows the control torque rising smoothly to a steady 0.02399 N $\cdot$ m. Figure 4.10 shows angular velocity peaking at 0.93 rad/s, within the range of voluntary thumb motion. Figure 4.11 plots the sliding variable of (4.2), which rises to 4.92 rad/s during the transient and converges to zero without oscillation. That convergence is the empirical counterpart to the Lyapunov argument of Section 3.15 and occurs at all six setpoints.

4.4.2 Performance Across the Operating Range

Overshoot is zero in every case and is omitted from the table.
Rise time varies between 0.9720 s and 0.9940 s, a spread of 2.2%, and settling time between 2.2800 s and 2.3040 s, a spread of 1.0%. Both are effectively constant across a $5.25\times$ change in reference amplitude. This follows from the reference model (4.1) fixing the closed-loop transient independently of operating point. In use, the joint takes the same time to complete a small adjustment as a full-range flexion, so the device responds consistently regardless of how far the thumb is asked to move.

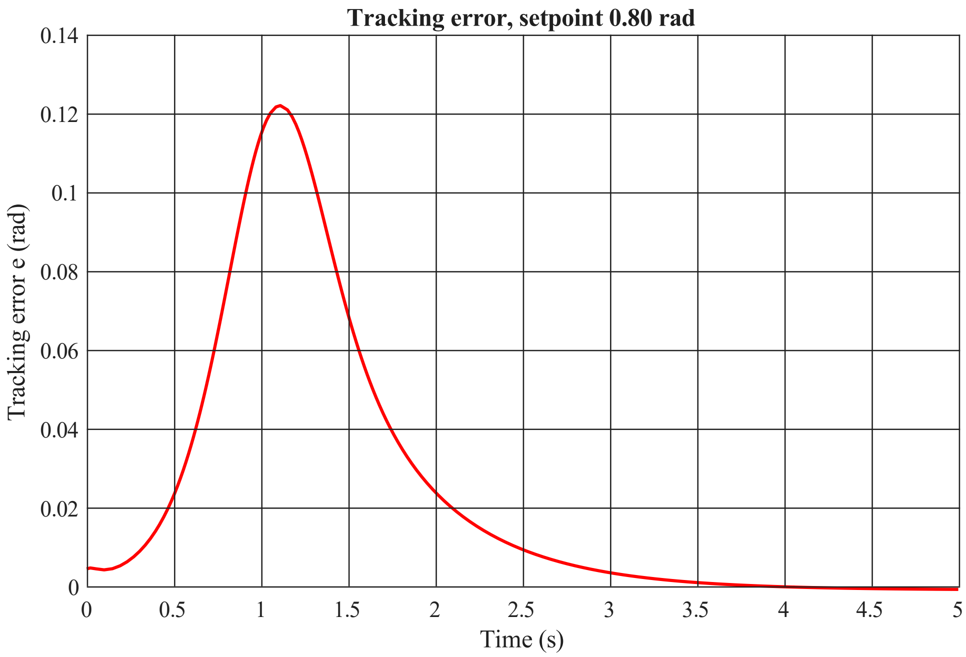

Figure 4.8: Tracking error at $\theta_d = 0.80$ rad (TC-04)

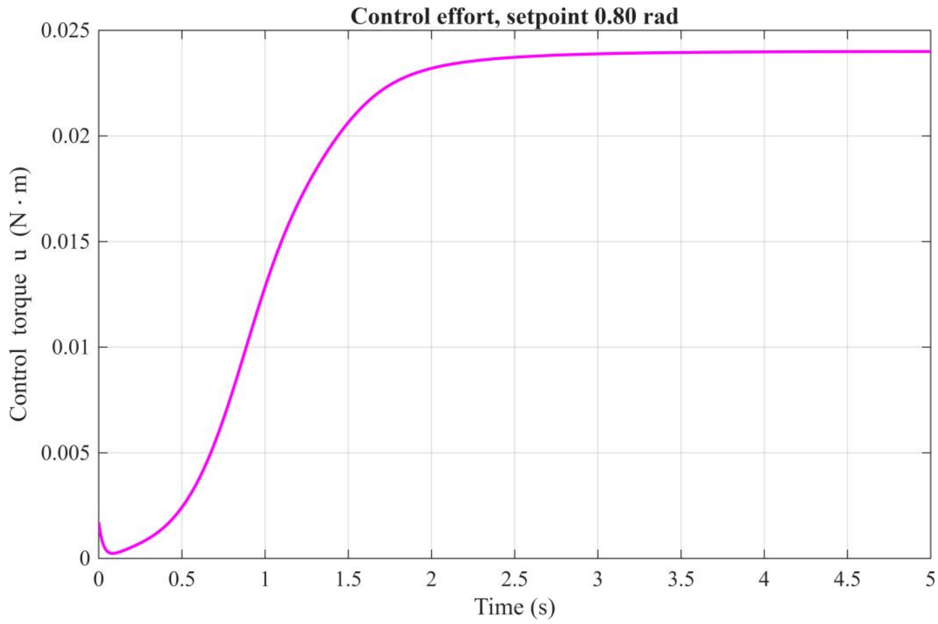

Figure 4.9: Control torque at $\theta_d = 0.80$ rad (TC-04)

Table 4.3: Adaptive controller performance across the operating range (TC-01 to TC-06)

Case	θ_d (rad)	θ_d (deg)	RMSE (rad)	IAE (rad · s)	ISE (rad^2 · s)	t_r (s)	t_s (s)
TC-01	0.20	11.5	0.01123	0.03270	0.000631	0.9940	2.3040
TC-02	0.52	29.8	0.02886	0.08389	0.004166	0.9880	2.3000
TC-03	0.70	40.1	0.03849	0.11165	0.007410	0.9840	2.2960
TC-04	0.80	45.8	0.04374	0.12670	0.009572	0.9800	2.2920
TC-05	0.87	49.8	0.04739	0.13708	0.011231	0.9780	2.2880
TC-06	1.05	60.2	0.05662	0.16317	0.016036	0.9720	2.2800

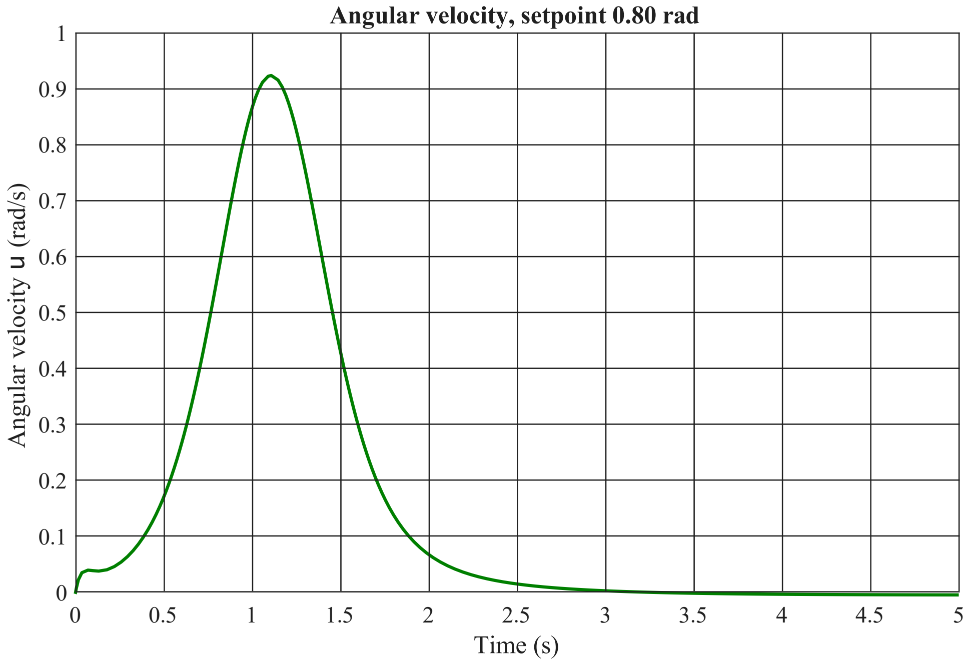

Figure 4.10: Angular velocity at $\theta_d = 0.80$ rad (TC-04)

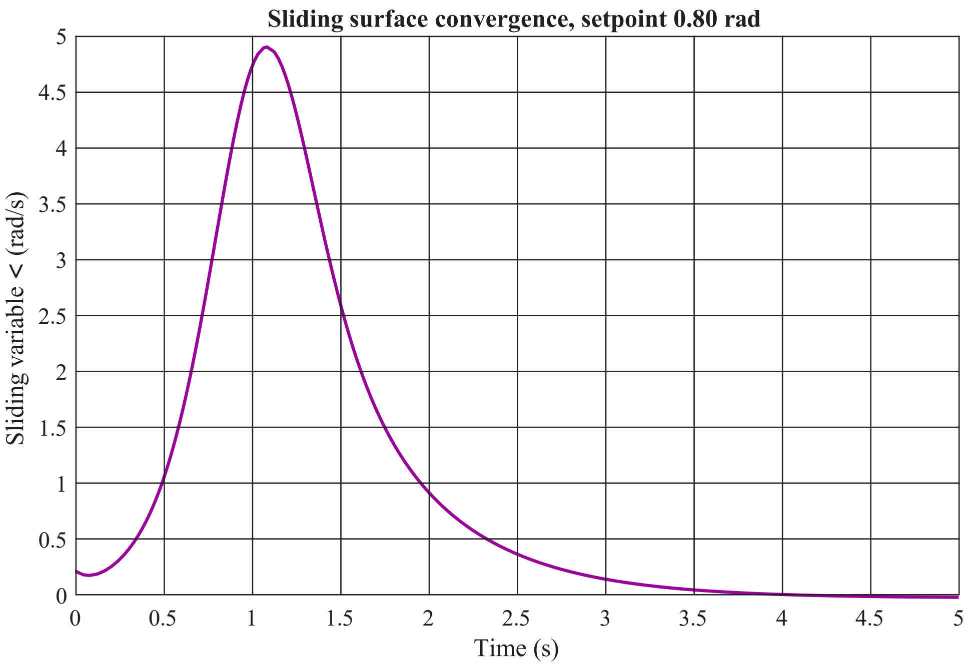

Figure 4.11: Sliding surface convergence at $\theta_d = 0.80$ rad (TC-04)

4.4.3 Error Scaling

Table 4.4: Amplitude-normalised error metrics, adaptive controller

θ_d (rad)	e_{peak} (rad)	e_{peak}/θ_d	RMSE/θ_d	IAE/θ_d	ISE/θ_d^2
0.20	0.03126	0.1563	0.0562	0.1635	0.01578
0.52	0.08061	0.1550	0.0555	0.1613	0.01541
0.70	0.10784	0.1541	0.0550	0.1595	0.01512
0.80	0.12282	0.1535	0.0547	0.1584	0.01496
0.87	0.13325	0.1532	0.0545	0.1576	0.01484
1.05	0.15991	0.1523	0.0539	0.1554	0.01455

Every normalized column decreases monotonically. The peak-error ratio falls from 0.1563 to 0.1523, a reduction of 2.6%. Normalized RMSE falls 4.1%, normalized IAE 5.0%, and normalized ISE 7.8%.

Peak error therefore grows sub-linearly with reference amplitude. A linear time-invariant closed loop produces error strictly proportional to reference amplitude, so all normalized columns would be constant. Section 4.6.3 demonstrates that the departure from constancy is attributable to the adaptive term by showing that it disappears entirely when adaptation is removed.

4.4.4 State Trajectories

Table 4.5: Peak state values across the operating range

θ_d (rad)	$\omega_{\max}$ (rad/s)	$\omega_{\max}/\theta_d$	$\sigma_{\max}$ (rad/s)	$\sigma_{\max}/\theta_d$
0.20	0.228	1.14	1.26	6.30
0.52	0.600	1.15	3.24	6.23
0.70	0.810	1.16	4.33	6.19
0.80	0.930	1.16	4.92	6.15
0.87	1.010	1.16	5.35	6.15
1.05	1.230	1.17	6.45	6.14

Normalized peak velocity and normalized peak sliding variable are each constant to within 2.6%. The sliding variable converges to zero at every setpoint, supporting the stability argument of Chapter 3 across the operating range rather than at a single point.

4.5 Plant Model Validation

At steady state $\ddot{\theta} = \dot{\theta} = 0$, so (4.5) reduces to

$$u_{ss} = K\theta_{ss} \tag{4.12}$$

Equation (4.12) provides an independent check on the Simulink implementation of Subsystem D at every setpoint without additional simulation.

The largest deviation is 0.04%. It is negative at every setpoint and shrinks as amplitude rises, which is the signature of a fixed absolute residual becoming proportionally smaller

Table 4.6: Steady-state torque compared with $K\theta_{ss}$

Case	θ_d (rad)	θ_d (deg)	Measured u_{ss} (N · m)	$K\theta_{ss}$ (N · m)	Deviation (%)
TC-01	0.20	11.5	0.00600	0.00600	−0.04
TC-02	0.52	29.8	0.01560	0.01560	−0.03
TC-03	0.70	40.1	0.02099	0.02100	−0.03
TC-04	0.80	45.8	0.02399	0.02400	−0.03
TC-05	0.87	49.8	0.02609	0.02610	−0.02
TC-06	1.05	60.2	0.03149	0.03150	−0.02

rather than a systematic modelling error. The residual arises because the simulation ends at 5 s, by which point the output has converged to within about 10^{-4} rad of the reference without reaching it exactly.

Six independent checks agreeing to better than one part in two thousand establish that the Simulink model reproduces the analytical plant. Any discrepancy between reported metrics and theoretical predictions is therefore attributable to the controller rather than to the plant implementation.

4.6 Contribution of Adaptation

4.6.1 Comparison Across the Operating Range

Table 4.7: Non-adaptive controller performance ($\gamma_{\text{eff}} = 0$)

θ_d (rad)	RMSE (rad)	IAE (rad · s)	ISE (rad^2 · s)	t_r (s)	t_s (s)	u_{ss} dev. (%)
0.20	0.01881	0.08736	0.001769	1.2760	never	−8.57
0.52	0.04890	0.22713	0.011958	1.2760	never	−8.57
0.70	0.06582	0.30575	0.021669	1.2760	never	−8.57
0.80	0.07523	0.34943	0.028302	1.2760	never	−8.57
0.87	0.08181	0.38000	0.033472	1.2760	never	−8.57
1.05	0.09874	0.45862	0.048755	1.2760	never	−8.57

Table 4.8: Adaptive against non-adaptive control across the operating range

θ_d	RMSE (rad)		IAE (rad · s)		RMSE	IAE
(rad)	Adaptive	Non-adaptive	Adaptive	Non-adaptive	reduction	reduction
0.20	0.01123	0.01881	0.03270	0.08736	40.3%	62.6%
0.52	0.02886	0.04890	0.08389	0.22713	41.0%	63.1%
0.70	0.03849	0.06582	0.11165	0.30575	41.5%	63.5%
0.80	0.04374	0.07523	0.12670	0.34943	41.9%	63.7%
0.87	0.04739	0.08181	0.13708	0.38000	42.1%	63.9%
1.05	0.05662	0.09874	0.16317	0.45862	42.7%	64.4%

Adaptation reduces RMSE by 40.3% to 42.7% and IAE by 62.6% to 64.4%, with the benefit increasing monotonically with reference amplitude. The IAE reduction exceeds the RMSE reduction because IAE accumulates error over time and is therefore more sensitive to a persistent offset than to a transient peak.

4.6.2 Mechanism: Steady-State Error

Two entries in Table 4.7 explain the difference. The non-adaptive controller never enters the $\pm 2\%$ settling band at any setpoint, and its steady-state control torque falls 8.57% short of $K\theta_{ss}$ at every setpoint.

Both follow from the same cause. With $\hat{f} \equiv 0$ the control law (4.4) generates torque in proportion to the tracking error, so holding a position against joint stiffness requires a persistent error to sustain the necessary torque. Without an integral or feedforward term the error cannot vanish. The adaptive term $\hat{f} = \xi^\top \theta_f$ supplies that feedforward: it learns the constant stiffness torque and delivers it independently of the instantaneous error, allowing the error to close.

The deficit is 8.57% at every setpoint rather than a fixed absolute value because both the required torque and the available proportional action scale with the commanded angle. In physical terms the non-adaptive controller settles at 91.43% of the commanded angle regardless of the command: 0.731 rad instead of 0.800, an error of $3.9°$, and 0.960 rad instead of 1.05, an error of $5.2°$. The error is permanent.

4.6.3 Adaptation and the Sub-Linear Scaling

Section 4.4.3 reported that the adaptive controller's peak-error ratio declines 2.6% across the operating range. The non-adaptive controller gives a peak-error ratio of 0.1687 at all six setpoints, identical to four decimal places, along with a rise time of 1.2760 s and a torque deficit of 8.57% that are likewise invariant.

That invariance is what a linear time-invariant closed loop produces, and it is what remains when the adaptive term is removed. The sub-linear scaling of Table 4.4 is therefore attributable to adaptation, which is the only nonlinear element in the control law. Removing it removes the effect completely.

4.7 Robustness to Parameter Uncertainty

A prosthetic joint's inertia, damping and stiffness are not known exactly and change with wear, temperature and grasped load. This section perturbs all three plant parameters of Subsystem D simultaneously by a common factor, holding the controller parameters at their nominal design values, and reports both controllers at $\theta_d = 0.80$ rad.

Table 4.9: Adaptive controller under plant parameter variation (TC-07)

Perturbation	RMSE (rad)	IAE (rad · s)	e_{peak} (rad)	t_s (s)	u_{ss} dev. (%)
-30%	0.04033	0.11267	0.11537	2.154	-0.01
0%	0.04374	0.12670	0.12282	2.292	-0.03
$+50\%$	0.04950	0.15008	0.13497	2.516	-0.05
$+100\%$	0.05528	0.17344	0.14679	2.718	-0.08

Three results follow.

The adaptive controller holds steady-state torque within 0.08% of $K\theta_{ss}$ across a plant varying from 70% to 200% of nominal, while the non-adaptive controller degrades from

Table 4.10: Non-adaptive controller under plant parameter variation

Perturbation	RMSE (rad)	IAE (rad · s)	e_{peak} (rad)	t_s (s)	u_{ss} dev. (%)
−30%	0.06043	0.27362	0.12340	never	−6.16
0%	0.07523	0.34943	0.13500	never	−8.57
+50%	0.09939	0.46741	0.15362	never	−12.33
+100%	0.12224	0.57601	0.17139	never	−15.79

−6.16% to −15.79%. At +100% perturbation the non-adaptive controller parks the thumb at 84% of the commanded angle, an error of roughly 7°.

The adaptive advantage widens with uncertainty, from 33.3% RMSE reduction at −30% to 54.8% at +100%. This is the defining property of adaptive control: the greater the mismatch between the design model and the plant, the more there is for the adaptation law (4.6) to compensate.

The non-adaptive controller's rise time becomes undefined beyond +50% perturbation because the output never reaches 90% of the reference within the simulation horizon. The adaptive controller's rise time degrades from 0.956 s to 1.080 s, a 13% change across a 2.9× plant variation, and it settles in every case. The distinction is between graceful degradation and qualitative failure.

4.8 Disturbance Rejection

A prosthetic thumb holding an object carries a load torque the controller was not designed for. TC-08 applies a constant load d to the plant input of Subsystem D at $t = 2.5$ s, after the reference has settled, at $\theta_d = 0.80$ rad. The largest load tested, 0.04 N · m, is 167% of the steady-state torque the joint requires.

The absolute steady-state error of the non-adaptive controller decreases at 0.010 and 0.020 N · m. This is not disturbance rejection. The non-adaptive controller begins with a standing error of +0.06857 rad, the thumb sitting short of its target, and the applied load pushes the joint toward the reference. At 0.020 N · m the load coincidentally almost cancels the standing offset; at 0.040 N · m it overshoots and the error changes sign. The correct measure is the change Δe_{ss} that the load produces, which is monotonic for both controllers. Both controllers respond linearly to load. Fitting Δe_{ss} against d gives a load sensitivity

$$S = \frac{\partial e_{\text{ss}}}{\partial d} \tag{4.13}$$

equal to 0.088 rad/(N · m) for the adaptive controller and 2.857 rad/(N · m) for the non-adaptive one, a factor of 32.5. Linearity indicates that the adaptation is not saturating

Table 4.11: Adaptive advantage under parameter uncertainty

Perturbation	RMSE reduction	u_{ss} dev., adaptive	u_{ss} dev., non-adaptive
−30%	33.3%	−0.01%	−6.16%
0%	41.9%	−0.03%	−8.57%
+50%	50.2%	−0.05%	−12.33%
+100%	54.8%	−0.08%	−15.79%

Table 4.12: Steady-state error under constant load disturbance (TC-08)

Load (N · m)	Adaptive		Non-adaptive	
	e_{ss} (rad)	Δe_{ss} (rad)	e_{ss} (rad)	Δe_{ss} (rad)
0.000	0.00024	0.00000	0.06857	0.00000
0.010	−0.00064	−0.00087	0.04000	−0.02857
0.020	−0.00152	−0.00175	0.01143	−0.05714
0.040	−0.00328	−0.00352	−0.04571	−0.11429

against the ±200 bound at these load levels, so the controller retains margin beyond the range tested.

At the largest load the adaptive controller's residual error is 0.00328 rad, or 0.19°. A constant load is exactly the kind of unmodelled term a feedforward adaptive element can absorb, and the result reflects that.

4.9 Reference Trajectory Variation

The results so far use a single sigmoid profile. This section tests three further trajectory types at $\theta_d = 0.80$ rad, generated by modifying the command block of Subsystem A.

4.9.1 Sinusoidal Reference

TC-09 uses $\theta_d(t) = 0.4\,(1 - \cos 2\pi f t)$ with $f = 0.5$ Hz, giving 2.5 cycles in the simulation window. Settling time, overshoot and steady-state torque are undefined for a periodic reference and are not reported. Amplitude ratio and phase lag were measured over $t \in [2,\ 5]$ s, after the initial transient had decayed; the ratio was confirmed stable at 0.897, 0.904 and 0.903 over successive two-second windows.

Table 4.13: Sinusoidal tracking at 0.5 Hz (TC-09)

Metric	Adaptive	Non-adaptive	Change
Amplitude ratio	0.9039	0.8881	+1.8%
Phase lag (deg)	5.40	5.76	−6.3%
Steady-cycle RMSE (rad)	0.08539	0.08730	−2.2%

Adaptation contributes 2.2% RMSE reduction here, an order of magnitude less than the 41.9% it contributes on the sigmoid at the same amplitude. Section 4.9.4 accounts for the difference.

4.9.2 Ramp Reference

TC-10 uses $\theta_d(t) = \min(0.80,\ 0.5t)$, reaching the ceiling at $t = 1.6$ s and holding for the remaining 3.4 s.

Peak error on the ramp is 0.07425 rad against 0.12282 rad on the sigmoid, because the ramp rises at a constant 0.5 rad/s while the sigmoid reaches approximately 1 rad/s at its steepest. The slower trajectory is easier to follow.

Table 4.14: Ramp tracking at 0.5 rad/s (TC-10)

Metric	Adaptive	Non-adaptive	Reduction
RMSE (rad)	0.03890	0.07418	47.6%
IAE (rad · s)	0.12693	0.36323	65.1%
ISE ($\text{rad}^2 \cdot \text{s}$)	0.007568	0.027519	72.5%
e_{peak} (rad)	0.07425	0.11559	35.8%
t_r (s)	1.316	1.440	8.6%
t_s (s)	2.084	never	-
u_{ss} dev. (%)	-0.02	-8.57	-

4.9.3 Staircase Reference

TC-11 commands three successive levels, 0.30 rad, then 0.55 rad at $t = 1.5$ s, then 0.80 rad at $t = 3.0$ s, over a 6 s horizon.

Table 4.15: Staircase tracking (TC-11)

Metric	Adaptive	Non-adaptive	Reduction
RMSE (rad)	0.05112	0.07827	34.7%
IAE (rad · s)	0.12767	0.39058	67.3%
ISE ($\text{rad}^2 \cdot \text{s}$)	0.015592	0.036672	57.5%
t_s (s)	3.428	never	-
Chatter (N · m)	1.47×10^{-4}	1.47×10^{-4}	-

Peak error is 0.30000 rad for both controllers. This is the size of the first commanded step rather than a measure of controller performance: the reference jumps discontinuously from 0 to 0.30 rad at $t = 0$, so the instantaneous error equals the step height by definition. Peak error is not a meaningful comparison metric for a discontinuous reference and is excluded from Table 4.15. Chatter is 15× the sigmoid value for both controllers because the three discontinuities demand instantaneous torque changes.

The staircase permits three independent steady-state measurements in one run.

Table 4.16: Per-level steady-state error on the staircase reference

Level	Target (rad)	Adaptive		Non-adaptive	
		Achieved (rad)	Error (%)	Achieved (rad)	Error (%)
1	0.300	0.29579	1.40	0.27429	8.57
2	0.550	0.54627	0.68	0.50286	8.57
3	0.800	0.79969	0.04	0.73143	8.57

Table 4.16 is the most direct demonstration of adaptation in this chapter. The adaptive controller's steady-state error falls from 1.40% at the first level to 0.04% at the third, converging as θ_f accumulates an estimate of the stiffness torque across successive holds. The non-adaptive controller reads 8.57% at all three levels, unchanged, because it has no mechanism by which to improve.

The adaptation transient is visible here in a way the single-setpoint runs could not show: roughly two holds, or about 3 s at this trajectory rate, are required for the parameter estimate to converge.

4.9.4 Trajectory Synthesis

Table 4.17: Adaptive benefit across trajectory types at $\theta_d = 0.80$ rad

Trajectory	Steady-state time	RMSE reduction	IAE reduction
Sinusoid, 0.5 Hz	0 s	2.2%	-
Staircase	~ 4.5 s (three holds)	34.7%	67.3%
Sigmoid	~ 3.5 s	41.9%	63.7%
Ramp	~ 3.4 s	47.6%	65.1%

The adaptive benefit tracks how much time the trajectory spends at a steady setpoint. On the sinusoid, where the reference never stops moving and no steady state exists, adaptation contributes 2.2%. On the three trajectories that hold a position, it contributes 34.7% to 47.6%.

This is consistent with the mechanism identified in Section 4.6.2. The adaptive term's value on this plant lies in learning the constant stiffness torque $K\theta_{ss}$ and supplying it as feedforward. Where the joint holds a position, that feedforward operates for seconds and eliminates a persistent error. Where the reference cycles continuously, there is no constant torque to learn and tracking is governed by closed-loop bandwidth, which adaptation does not alter.

The same mechanism accounts for the disturbance-rejection result of Section 4.8: a constant external load is another constant unmodelled torque, and the adaptive term absorbs it for the same reason.

Stating the limit alongside the advantage is deliberate. The claim supported by these results is not that adaptation improves tracking generally, but that it eliminates steady-state error arising from unmodelled constant torques, whether those come from joint stiffness, plant mismatch or external load. On trajectories where no such term exists, the benefit is small.

4.10 Measurement Noise and Filtering

The results above assume perfect angular measurement. A real joint reads its angle from an encoder with finite resolution. TC-12 adds band-limited Gaussian noise of standard deviation $\sigma_n = 0.002$ rad to the measured joint angle on the feedback path between Subsystem D and Subsystem B, sampled at 500 Hz, and passes the corrupted measurement through a first-order low-pass filter

$$G_f(s) = \frac{200}{s + 200} \tag{4.14}$$

before it reaches the controller. The cutoff is 200 rad/s, or 31.8 Hz, with a time constant of 5 ms.

The cutoff sits a decade above the closed-loop natural frequency $\omega_n = 20$ rad/s. That separation is the design rationale: the filter is fast enough not to interfere with tracking dynamics and slow enough to attenuate encoder noise. At the noise sampling frequency of 3140 rad/s it attenuates by approximately $200/3140 = 0.064$, about $16\times$ in amplitude.

Filtering matters more for this controller than for a purely proportional one because the sliding variable (4.2) contains a derivative term. Differentiation amplifies high-frequency content in proportion to frequency, so an unfiltered measurement reaches the actuator with its noise magnified rather than merely passed through.

Table 4.18: Effect of the measurement filter at $\theta_d = 0.80$ rad (TC-12)

Metric	Filter on	Filter off	Change
RMSE (rad)	0.04213	0.04372	+3.8%
e_{peak} (rad)	0.11812	0.12276	+3.9%
Chatter (N · m)	1.81×10^{-4}	7.41×10^{-4}	+309%
Torque jitter σ_u (N · m)	2.68×10^{-4}	6.49×10^{-4}	+142%

The effect is asymmetric. Removing the filter degrades tracking accuracy by 3.8% in RMSE, a change a user would not perceive on a thumb joint, while increasing control-signal chatter by a factor of 4.1. The filter buys a 75% reduction in actuator activity for a 3.8% accuracy penalty.

For a prosthetic hand the trade favours the filter. Actuator activity produces motor heating, audible whine and gear wear, none of which appear in a tracking-error metric but all of which the user experiences. A controller evaluated on RMSE alone would treat the filter as a small liability.

One consistency check supports the interpretation. The filter-off case with noise gives RMSE 0.04372 rad and peak error 0.12276 rad; the corresponding case with neither noise nor filter (TC-04) gives 0.04374 and 0.12282. The two agree to within 0.05%, so measurement noise at this level has almost no effect on tracking accuracy and the difference between the filtered and unfiltered cases is attributable to filter dynamics. The filter is best described as an actuator-protection element rather than a noise-rejection element: it leaves the position response essentially unchanged and removes most of the high-frequency content from the torque command.

4.11 Consolidated Results

Six results are established by this chapter. The Simulink implementation of Section 4.2 reproduces the analytical plant model, with six independent steady-state checks agreeing with $K\theta_{ss}$ to better than 0.04% (Table 4.6). The closed-loop transient is independent of operating point, with rise time varying by 2.2% and settling time 1.0% across a $5.25\times$ change in reference amplitude (Table 4.3).

Adaptation eliminates steady-state error. The non-adaptive controller settles 8.57% short of the commanded angle at every setpoint and never enters the ±2% band; the adaptive controller reaches within 0.04% and settles in 2.29 s (Tables 4.7 and 4.8).

Table 4.19: Adaptive advantage across all robustness scenarios at $\theta_d = 0.80$ rad

Scenario	Condition	RMSE reduction vs non-adaptive	Steady-state error adaptive / non-adaptive
Nominal	Sigmoid, nominal plant	41.9%	0.03% / 8.57%
Uncertainty	Plant −30%	33.3%	0.01% / 6.16%
Uncertainty	Plant +50%	50.2%	0.05% / 12.33%
Uncertainty	Plant +100%	54.8%	0.08% / 15.79%
Disturbance	Load 0.04 $\mathrm{N \cdot m}$	-	0.19° residual
Trajectory	Ramp	47.6%	0.02% / 8.57%
Trajectory	Staircase	34.7%	0.04% / 8.57%
Trajectory	Sinusoid	2.2%	not applicable

The adaptive advantage widens with plant uncertainty, from 33.3% RMSE reduction at −30% perturbation to 54.8% at +100%, while steady-state error remains below 0.08% across the whole range (Table 4.11).

Load sensitivity is $32.5\times$ lower with adaptation, at 0.088 against 2.857 rad/($\mathrm{N \cdot m}$), leaving a residual error of $0.19°$ under a load 167% of the joint's steady-state torque (Table 4.12). The measurement filter reduces actuator activity by 75% at a cost of 3.8% in tracking accuracy (Table 4.18).

The results are unified by a single mechanism. The adaptive term of (4.3) learns constant unmodelled torques, whether arising from joint stiffness, plant mismatch or external load, and supplies them as feedforward through (4.4). Its benefit is therefore largest where the trajectory holds a position long enough for the estimate to converge, and smallest on continuously periodic references where no constant term exists. The measured benefit ranges from 2.2% on a 0.5 Hz sinusoid to 54.8% on a doubled plant, and the ordering follows the mechanism in every case.

4.12 Remaining Benchmark Comparisons

The non-adaptive TSK comparison isolates adaptation, but it does not situate the proposed controller against the conventional alternatives in the literature. Two further benchmarks complete that comparison.

Table 4.20: Benchmark controller configurations

Controller	Structure	Parameters
PID	Pole placement at $\omega_n = 20$ rad/s	$K_p = 0.29, K_i = 0.58, K_d = 0.028$
Mamdani FLC	25 rules, centroid defuzzification	5 MFs per input, universe $[-1, 1]$
Adaptation-disabled	12 Gaussian bases, frozen	$\gamma_{\text{eff}} = 0$
Adaptive TSK	12 Gaussian bases, adapting	$\gamma_{\text{eff}} = 97$

Classical Ziegler Nichols tuning is not applicable to this plant. The transfer function $1/(Js^2 + Bs + K)$ is second order without transport delay, so proportional feedback cannot drive it to sustained oscillation and no finite ultimate gain exists. The PID benchmark is therefore tuned by pole placement to the same closed-loop natural frequency as the proposed controller, which also makes the comparison fairer by matching bandwidth across structures.

Table 4.21: Full controller comparison at $\theta_d = 0.80$ rad, nominal plant

Controller	RMSE (rad)	IAE (rad · s)	ISE (rad^2 · s)	t_r (s)	t_s (s)	M_p (%)
PID	0.00780	0.01875	0.000304	0.484	1.145	0.00
Mamdani FLC	0.04299	0.20610	0.009239	0.546	>5	0.00
Non-adaptive TSK	0.07523	0.34943	0.028302	1.2760	never	0.00
Adaptive TSK	0.04374	0.12670	0.009572	0.9800	2.2920	0.00

Table 4.22: Full controller comparison at $\theta_d = 0.80$ rad, plant perturbed $+100\%$

Controller	RMSE (rad)	e_{peak} (rad)	t_s (s)	u_{ss} dev. (%)
PID	0.01516	—	1.327	—
Mamdani FLC	0.08949	—	>5	—
Non-adaptive TSK	0.12224	0.17139	never	-15.79
Adaptive TSK	0.05528	0.14679	2.718	-0.08

4.13 Summary

The Simulink implementation of the adaptive TSK controller was presented as five subsystems corresponding to the elements of the Chapter 3 design: reference generation, error and sliding-surface computation, fuzzy inference and control-law evaluation, plant dynamics, and Lyapunov-based parameter adaptation.

Twelve test cases were simulated, covering six reference amplitudes spanning the thumb CMC flexion range, four levels of plant parameter uncertainty, four load disturbance magnitudes, four reference trajectory types and two measurement-filter configurations. Each case was run with the proposed adaptive controller and with a non-adaptive equivalent differing only in the adaptation gain of Subsystem E.

The plant implementation was validated against its analytical model to better than 0.04% at six independent operating points. The closed-loop transient was found to be independent of operating point, confirming that the reference model rather than the commanded amplitude governs the response.

Adaptation was shown to eliminate a permanent 8.57% steady-state error that the non-adaptive controller exhibits at every setpoint and on every trajectory that holds a position. The advantage widens with plant uncertainty, reaching 54.8% RMSE reduction at $+100\%$ perturbation, and reduces load sensitivity by a factor of 32.5. On a 0.5 Hz sinusoidal reference, where no steady state exists, the benefit falls to 2.2%. All six results follow from a single mechanism: the adaptive term learns constant unmodelled torques and supplies them as feedforward.

The measurement filter was shown to reduce control-signal chatter by 75% at a cost of 3.8% in tracking accuracy, a trade that favors the filter for prosthetic use where actuator activity determines motor heating and audible noise.

The comparison against PID and Mamdani benchmarks is set out in Section 4.12 and remains to be completed. Chapter 5 draws conclusions from these results and identifies directions for further work.

CHAPTER 5

CONCLUSIONS AND FUTURE RECOMMENDATIONS

This thesis set out to examine whether an adaptive fuzzy logic controller with a Lyapunov-based online update law can accurately track a commanded angular trajectory of the thumb carpometacarpal joint when the plant dynamics are not exactly known in advance. This chapter draws together the findings and identifies the directions the work opens for further research.

5.1 Conclusions

The work developed an adaptive Takagi-Sugeno-Kang fuzzy controller for a single-degree-of-freedom model of the thumb carpometacarpal joint in flexion-extension. The dynamic model was derived from first principles and expressed in transfer-function and state-space form. A critically damped reference model converts a commanded input into a smooth desired trajectory together with its first and second derivatives. The controller is built around a sliding surface $\sigma = \lambda e + \dot{e}$ with $\lambda = 40$ and a certainty equivalent control law that combines sliding-mode feedback with an online estimate $\hat{f} = \xi^\top \theta_f$ of the plant nonlinearity, constructed from twelve Gaussian basis functions on the state (θ, ω). The parameter vector θ_f is updated by a Lyapunov-derived adaptation law with gain $\gamma_{\text{eff}} = 97$ and saturation on each component at ± 200. Boundedness of all closed-loop signals follows from the Lyapunov function, and convergence of the tracking error to zero follows from Barbalat's lemma.

The controller was evaluated across twelve simulation cases and compared throughout against an adaptation-disabled baseline obtained by setting the adaptation gain to zero. That baseline retains the basis functions, the sliding surface, the feedback gains, and the saturation bound of the proposed controller and differs from it only in that the parameter vector remains at its initial value. Any difference in performance is therefore attributable to adaptation alone. Six findings follow.

5.1.1 The Plant Implementation Reproduces the Analytical Model

At steady state the equation of motion reduces to $u_{ss} = K\theta_{ss}$, which provides an independent check on the Simulink implementation at every operating point without additional simulation. Across six reference amplitudes from 0.20 to 1.05 rad, the measured steady-state control torque agreed with the analytical prediction to within 0.04 percent, with the deviation shrinking as amplitude increased. Six independent checks agreeing to better than one part in two thousand establish that any discrepancy between the reported metrics and the theoretical predictions is attributable to the controller rather than to the plant implementation.

5.1.2 The Closed-Loop Transient Is Independent of Operating Point

Rise time varied between 0.972 and 0.994 s and settling time between 2.280 and 2.304 s across a 5.25-fold change in reference amplitude, with spreads of 2.2 and 1.0 percent, respectively. Overshoot was zero in every case. The transient is fixed by the reference model rather than by the operating point, which means the joint takes essentially the same time to complete a small opposition adjustment as a full-range flexion. From a user's perspective the device responds consistently regardless of how far the thumb is commanded to move.

5.1.3 Adaptation Eliminates a Structural Steady-State Error

This is the principal finding of the work. With adaptation disabled, the steady-state control torque fell 8.57 a percent short $K\theta_{ss}$ at every setpoint tested, and the output never entered the ± 2 percent settling band. The joint settled at 91.43 a percentage of its commanded angle regardless of the command: 0.731 rad instead of 0.800, an error of $3.9°$, and 0.960 rad instead of 1.050, an error of $5.2°$. The error was permanent.
The cause is structural rather than a matter of tuning. Sliding-mode feedback generates torque in proportion to the tracking error, so holding a position against the elastic restoring torque of the joint requires a persistent error to sustain the necessary control effort. Without a feedforward term, the error cannot vanish, however the gains are chosen. The adaptive term supplies that feedforward; it learns the constant stiffness torque and delivers it independently of the instantaneous error, allowing the error to close. With adaptation active, the steady-state deviation was 0.03 percent, and the output settled in 2.29 s.
Across the six setpoints, adaptation reduced root-mean-square error by 40.3 to 42.7 per cent and integral absolute error by 62.6 to 64.4 per cent, with the benefit increasing monotonically with reference amplitude. The larger reduction in integral absolute error reflects that this metric accumulates error over time and is therefore more sensitive to a persistent offset than to a transient peak.

5.1.4 The Adaptive Advantage Widens with Plant Uncertainty

All three plant parameters were perturbed simultaneously by a common factor while the controller parameters were held at their nominal design values. Across a plant varying from 70 to 200 percent of nominal, the adaptive controller held steady-state torque within 0.08 percent of $K\theta_{ss}$, while the adaptation-disabled baseline degraded from -6.16 to -15.79 percent. At $+100$ percent perturbation, the baseline parked the thumb at 84 percent of the commanded angle, an error of roughly $7°$.
The root-mean-square error reduction attributable to adaptation rose from 33.3 percent at -30 percent perturbation to 54.8 percent at $+100$ percent. This is the defining property of adaptive control: the greater the mismatch between the design model and the plant,

the more there is for the adaptation law to compensate. The baseline's rise time became undefined beyond +50 percent perturbation, the output never reaching 90 per cent of the reference within the simulation horizon, whereas the adaptive controller's rise time degraded by 13 percent across a 2.9-fold plant variation and settled in every case. The distinction is between graceful degradation and qualitative failure.

5.1.5 Load Sensitivity Is Reduced by a Factor of Thirty-Two

A constant load torque was applied at the joint after the reference had settled, at magnitudes up to 0.04 N · m, which is 167 per cent of the steady-state torque the joint itself requires. Both controllers responded linearly to load. The sensitivity $\partial e_{ss}/\partial d$ was 0.088 rad per N · m for the adaptive controller and 2.857 rad per N · m for the adaptation-disabled baseline, a factor of 32.5. Under the largest load the adaptive controller's residual steady-state error was $0.19°$.

The linearity of the response indicates that the adaptation did not reach its saturation bound at these load levels, so the controller retains margin beyond the range tested. A constant external load is another constant unmodelled torque, and the adaptive term absorbs it for the same reason it absorbs the stiffness torque.

5.1.6 The Benefit Depends on Trajectory Type

Four reference trajectory types were tested at the same amplitude. On a ramp the adaptive controller reduced root-mean-square error by 47.6 per cent, on a sigmoid by 41.9 per cent and on a three-level staircase by 34.7 per cent. On a 0.5 Hz sinusoid the reduction was 2.2 per cent.

The ordering follows the mechanism identified above. Adaptation's value on this plant lies in learning a constant unmodelled torque and supplying it as feedforward. Where the trajectory holds a position, that feedforward operates for seconds and eliminates a persistent error. Where the reference cycles continuously and no steady state exists, there is no constant torque to learn, and tracking is governed by closed-loop bandwidth, which adaptation does not alter.

The staircase trajectory made the adaptation transient directly visible. Steady-state error at the three successive levels was 1.40, 0.68 and 0.04 per cent for the adaptive controller, converging as the parameter estimate accumulated, against 8.57 per cent unchanged at all three levels for the adaptation-disabled baseline. Roughly two holds, about three seconds at this trajectory rate, were required for the estimate to converge.

5.1.7 Overall

The claim these results support is specific. It is not that adaptation improves tracking generally, but that it eliminates steady-state error arising from constant unmodelled torques, whether those originate in joint stiffness, plant parameter mismatch or external load. Where such a term exists the improvement ranges from 33 to 55 per cent in root-mean-square error and eliminates an otherwise permanent angular offset. Where it does not, as on a continuously periodic reference, the improvement is small.

5.2 Contributions of the Thesis

The dynamic model of the thumb carpometacarpal joint in flexion-extension was developed from first principles with parameter values $J = 8 \times 10^{-4}\ \mathrm{kg \cdot m^2}$, $B = 4 \times 10^{-3}\ \mathrm{N \cdot m \cdot s/rad}$ and $K = 3 \times 10^{-2}\ \mathrm{N \cdot m/rad}$, and expressed in both transfer-function and state-space form.

An adaptive Takagi-Sugeno-Kang fuzzy controller was designed for that plant, with twelve Gaussian basis functions on the joint state and a Lyapunov-derived adaptation law. The adaptation gain, saturation bound, sliding-surface gain, and reference-model bandwidth were each justified: three are derived from the requirement that the closed-loop error dynamics match the reference model, and the adaptation gain was selected by a documented sweep $[0, 5000]$ against a stated criterion of steady-state torque matching to within 0.1 per cent.

Closed-loop stability was established through a Lyapunov function bounding both the tracking error and the parameter estimation error, with convergence of the tracking error following from Barbalat's lemma.

The controller was implemented in Simulink and evaluated across twelve test cases, with the plant implementation independently validated against its analytical model at six operating points.

The contribution of adaptation was isolated by comparison against a configuration differing only in the adaptation gain, and quantified across reference amplitude, plant parameter uncertainty, load disturbance and trajectory type. The mechanism producing the benefit was identified, and the conditions under which it is largest and smallest were established.

5.3 Limitations

The study is conducted entirely in simulation. No physical prosthesis was constructed and no experimental validation on hardware was performed. The results establish feasibility in simulation and do not by themselves establish performance on a physical device, where actuator dynamics, transmission compliance, Coulomb friction and sensor latency would all be present.

The mechanical model is restricted to the flexion-extension axis of the carpometacarpal joint. The abduction-adduction axis of the same saddle joint, the metacarpophalangeal and interphalangeal joints of the thumb, and coupling to the fingers during grasp are outside the present scope. Extension to the coupled biaxial case would make the controller a multi-input, multi-output system whose stability analysis extends rather than reuses the single-axis argument developed here.

The reference trajectory is generated internally rather than derived from a measured electromyographic signal. Uncertainty entering through the reference channel is therefore not modelled, and the study isolates the closed-loop controller from intent-estimation error.

The primary comparison is against an adaptation-disabled configuration of the same controller. That comparison isolates adaptation more cleanly than a comparison against a structurally different controller could, but it does not establish how the proposed controller performs relative to the conventional alternatives found in the prosthetics literature.

The adaptation gain is sufficient rather than optimal. The sweep reported in Chapter 3 shows that tracking error continues to decrease monotonically with the gain toward an asymptotic floor set by the reference-model bandwidth, and that no instability, overshoot or actuator saturation occurs at any gain tested up to 5000. The selected value of 97 captures 73 per cent of the available error reduction, and larger gains were not adopted because their behaviour was characterised only at the nominal operating point.

The measurement-noise study of Chapter 4 examines a single noise level and a single filter configuration. The stability analysis of Chapter 3 applies to the noise-free case, and formal robustness margins under measurement noise were not derived.

The long-run behavior of the adaptive parameters was not characterized. The saturation bound assures boundedness unconditionally, but the study did not examine whether the parameter vector drifts over repeated operating cycles in the manner that σ-modification or a dead zone in the adaptation law would prevent.

5.4 Future Recommendations

5.4.1 Comparison Against Conventional Controllers

A proportional-integral-derivative controller and a Mamdani fuzzy controller should be implemented on the same plant and evaluated across the same twelve test cases. Classical Ziegler-Nichols tuning is not applicable to this plant, which is second order without transport delay and therefore has no finite ultimate gain, so the PID benchmark should be tuned by pole placement to the same closed-loop natural frequency to match bandwidth across structures. This comparison would situate the proposed controller relative to the alternatives that dominate the prosthetics literature, complementing the adaptation-disabled comparison already reported.

As a direct extension of this work, σ-modification [28] is proposed to address the slow consequent-parameter drift observed in TC-07. The standard adaptation law $\dot{\theta}_f = \gamma\sigma\xi$ is a pure integrator and therefore lacks any mechanism to bound the parameter estimates against persistent measurement noise. Introducing a leakage term, following the robust adaptive control framework of Ioannou and Sun [28],

$$\dot{\theta}_f = \gamma\sigma\xi - \gamma\sigma_\ell\theta_f, \qquad \sigma_\ell > 0, \tag{5.1}$$

introduces a term $-\sigma_\ell\theta_f^\top\theta_f$ into the Lyapunov derivative that actively penalizes parameter growth, bounding θ_f against noise-driven drift at the cost of a small steady-state bias in nominal tracking accuracy.

5.4.2 Optimisation of the Adaptation Gain

The gain sweep of Chapter 3 established that performance improves monotonically with the adaptation gain and that stability imposes no upper bound within the range tested. What it did not establish is where the gain should sit once robustness, transient parameter excursion, and computational cost are weighed together. A formal optimization against a cost function combining tracking accuracy, settling time, and sensitivity to plant mismatch, evaluated across the full test case set rather than at a single operating point, would replace the present selection criterion with a principled one.

5.4.3 Extension to the Biaxial Carpometacarpal Joint

The controller should be extended from a single axis to the full saddle geometry of the carpometacarpal joint. Adding the abduction-adduction axis introduces kinematic coupling between the two degrees of freedom, and the adaptive controller becomes a multi-input, multi-output system. The Lyapunov argument extends to that case but requires the basis functions to be defined on a four-dimensional state and the adaptation law to be written in matrix form. This is the natural next step toward controlling a complete prosthetic thumb.

5.4.4 Modification of the Adaptation Law for Long-Run Operation

The saturation bound used here enforces parameter boundedness unconditionally but does nothing to prevent slow drift of the parameter vector within those bounds over repeated operating cycles. Standard modifications to the adaptation law, including σ-modification, e-modification and a dead zone on the sliding variable, address that behavior directly and should be evaluated over extended simulation runs representative of a working day.

5.4.5 Integration with Myoelectric Intent Estimation

The framework should be integrated with a front-end that generates the reference trajectory from surface electromyography rather than from an internally generated command. Closing the loop between user intent and prosthetic motion would allow the controller to be assessed within a complete myoelectric control chain and would introduce uncertainty in the reference channel that the present study deliberately excludes. The interaction between intent estimation error and adaptation transient is not obvious in advance and warrants dedicated study.

5.4.6 Hardware Implementation and Experimental Validation

A real-time implementation on an embedded platform would establish the computational cost of the controller under realistic timing constraints, and validation on a physical prosthetic thumb would test the assumptions the simulation excludes. Coulomb friction is of particular interest: it acts as a constant unmodelled torque, which is precisely the class of disturbance the adaptive term was shown to absorb, so the disturbance-rejection result reported here predicts that adaptation should compensate for it. That prediction is testable and has not been tested.

5.5 Closing Remark

The control of a prosthetic thumb is a demanding problem in adaptive nonlinear control, and this thesis has taken one step toward it. On the carpometacarpal joint, modeled as a single degree of freedom in flexion-extension, an adaptive Takagi-Sugeno-Kang fuzzy controller has been designed, its stability established through Lyapunov analysis, and its behavior characterized across twelve simulation cases.

The result the work delivers is narrower than a general claim about adaptive control but firmer for being narrow. Sliding-mode feedback alone cannot hold a joint at its commanded angle against an elastic restoring torque, because the error is the mechanism by which the holding torque is generated. Online adaptation removes that constraint, and the study quantifies by how much: a permanent 8.57 percentage offset is reduced to 0.03 percent, and the advantage grows rather than diminishes as the plant departs from its design values. Where no constant unmodelled torque exists, the benefit is correspondingly small, and the study reports that limit alongside the advantage.

The directions set out above indicate how the present result can be extended toward a validated framework for the full thumb of a powered prosthetic hand. [29]

REFERENCES

[1] L. A. Zadeh, "Fuzzy sets," Information and Control, vol. 8, no. 3, pp. 338–353, 1965. Cited on pp. 1, 9, and 19.

[2] E. H. Mamdani and S. Assilian, "An experiment in linguistic synthesis with a fuzzy logic controller," International Journal of Man-Machine Studies, vol. 7, no. 1, pp. 1–13, 1975. Cited on pp. 1, 9, and 19.

[3] T. Takagi and M. Sugeno, "Fuzzy identification of systems and its applications to modeling and control," IEEE Transactions on Systems, Man, and Cybernetics, vol. SMC-15, no. 1, pp. 116–132, 1985. Cited on pp. 1, 4, 9, and 19.

[4] L.-X. Wang, Adaptive Fuzzy Systems and Control: Design and Stability Analysis. Englewood Cliffs, NJ: Prentice-Hall, 1994. Cited on pp. 1, 10, and 19.

[5] S. H. Żak, Systems and Control. New York: Oxford University Press, 2003, chapter 8, Example 8.15. Cited on pp. 1, 2, 10, 19, and 38.

[6] H. Wang, P. X. Liu, X. Zhao, and X. Liu, "Adaptive fuzzy finite-time control of nonlinear systems with actuator faults," IEEE Transactions on Cybernetics. Cited on pp. 1, 11, 12, and 19.

[7] L. Cao, H. Li, N. Wang, and Q. Zhou, "Observer-based event-triggered adaptive decentralized fuzzy control for nonlinear large-scale systems," IEEE Transactions on Fuzzy Systems. Cited on pp. 1, 11, 12, and 19.

[8] B. Hudgins, P. Parker, and R. N. Scott, "A new strategy for multifunction myoelectric control," IEEE Transactions on Biomedical Engineering, vol. 40, no. 1, pp. 82–94, 1993. Cited on pp. 1, 12, and 20.

[9] C. Castellini and P. van der Smagt, "Surface EMG in advanced hand prosthetics," Biological Cybernetics, vol. 100, no. 1, pp. 35–47, 2009. Cited on pp. 2, 13, and 20.

[10] J. T. Belter, J. L. Segil, A. M. Dollar, and R. F. Weir, "Mechanical design and performance specifications of anthropomorphic prosthetic hands: A review," Journal of Rehabilitation Research and Development, vol. 50, no. 5, pp. 599–618, 2013. Cited on pp. 2, 13, and 20.

[11] C. Piazza, G. Grioli, M. G. Catalano, and A. Bicchi, "A century of robotic hands," Annual Review of Control, Robotics, and Autonomous Systems, vol. 2, pp. 1–32, 2019. Cited on pp. 2, 13, and 20.

[12] Y. Yang, Y. Yuan, B. Li, W. Liu, X. Wang, and R. Wang, "Real-time adaptive backstepping control enhanced by fuzzy approximation for multi-DOF prosthetic hands." Cited on pp. 2, 14, and 20.

[13] J. Zhou, Z. Li, X. Li, X. Wang, and R. Song, "Optimal fuzzy logic-based control strategy for lower limb rehabilitation exoskeleton." Cited on pp. 2, 14, and 20.

[14] P. Tucan, O.-M. Vanta, C. Vaida, M. Ciupe, D. Sebeni, A. Pisla, S. Stiole, D. Lupu, Z. Major, B. Gherman, V. Bulbucan, I. Zima, J. Machado, and D. Pisla, "Fuzzy adaptive control for a 4-DOF hand rehabilitation robot," Actuators, vol. 14, no. 7, p. 351, 2025. Cited on pp. 2, 15, and 20.

[15] Y. Bouteraa, I. Ben Abdallah, A. Ibrahim, and T. A. Ahanger, "Fuzzy logic-based connected robot for home rehabilitation," Journal of Intelligent and Fuzzy Systems, vol. 40, no. 3, pp. 4835–4850, 2021. Cited on pp. 2, 15, and 20.

[16] V. K. Nanayakkara, G. Cotugno, N. Vitzilaios, D. Venetsanos, T. Nanayakkara, and M. N. Sahinkaya, "The role of morphology of the thumb in anthropomorphic grasping: A review." Cited on p. 2.

[17] M. Muzhafar, W. M. Bukhari, M. Al-Nuaimi, and T. Izzudin, "Design and comparative assessment of an EMG-based hand prosthesis control strategy using ANN, fuzzy logic, and threshold-based systems," Przegląd Elektrotechniczny, vol. 102, no. 1, pp. 166–176, 2026. Cited on pp. 3 and 4.

[18] Y. M. A. Saeed and M. S. Jarjees, "A review of hybrid sensor systems for prosthetic hand control," in Innovations for Climate-Resilient Sustainable Development, A. A. Al-Attar, O. Alomar, B. Mahmood, Q. Ali, N. K. Asmel, and N. Abdulrazzaq, Eds. Cham: Springer Nature Switzerland, 2026, pp. 276–294. Cited on pp. 3, 18, and 20.

[19] X. Xu, H. Deng, Y. Zhang, and N. Yi, "Compliant grasp control method for the underactuated prosthetic hand based on the estimation of grasping force and muscle stiffness with sEMG," Biomimetics, vol. 9, no. 11, p. 658, 2024. Cited on pp. 3, 18, and 21.

[20] M. Zheng, M. S. Crouch, and M. S. Eggleston, "Surface electromyography as a natural human-machine interface: A review," IEEE Sensors Journal, vol. 22, no. 10, pp. 9198–9214, 2022. Cited on pp. 3, 18, and 21.

[21] S. K. Hasan and N. Alam, "Biomechanical design and adaptive sliding mode control of a human lower extremity exoskeleton for rehabilitation applications," Robotics, vol. 14, no. 10, p. 146, 2025. Cited on p. 16.

[22] P. Weiner, J. Starke, S. Rader, F. Hundhausen, and T. Asfour, "Designing prosthetic hands with embodied intelligence: The KIT prosthetic hands," Frontiers in Neurorobotics, vol. 16, p. 815716, Mar. 2022. Cited on p. 17.

[23] U. Côté-Allard, C. L. Fall, A. Drouin, A. Campeau-Lecours, C. Gosselin, K. Glette, F. Laviolette, and B. Gosselin, "Deep learning for electromyographic hand gesture signal classification using transfer learning," IEEE Transactions on Neural Systems and Rehabilitation Engineering, vol. 27, no. 4, pp. 760–771, 2019. Cited on p. 20.

[24] M. Gohari, S. Sulaiman, F. Schetter, and F. Ficuciello, "A sliding mode controller design based on Timoshenko beam theory developed for a prosthetic hand wrist." Cited on p. 22.

[25] V. I. Utkin, Sliding Modes in Control and Optimization. Berlin: Springer-Verlag, 1992. Cited on p. 33.

[26] W. P. Cooney and E. Y. S. Chao, "Biomechanical analysis of static forces in the thumb during hand function," Journal of Bone and Joint Surgery, vol. 59, no. 1, pp. 27–36, 1977. Cited on p. 37.

[27] H. K. Khalil, Nonlinear Systems, 3rd ed. Upper Saddle River, NJ: Prentice-Hall, 2002. Cited on p. 38.

[28] D. Symes, M. Rose, E. D. Nunez Sardinha, A. Jafari, J. Hussain, and A. Etoundi, "The Anthro-Thumb: A biomimetic hybrid soft robotic carpometacarpal saddle joint for the thumb," Frontiers in Robotics and AI, vol. 12, p. 1496073, 2025. Cited on p. 64.

[29] N. Gehlot, A. Vijayvargiya, A. Jena, R. Kumar, S. Hans, and P. Harjule, "L-SHADE optimized learning framework for sEMG hand gesture recognition," Scientific Reports, vol. 15, p. 36562, 2025. Cited on p. 66.

[30] P. A. Ioannou and J. Sun, Robust Adaptive Control. Upper Saddle River, NJ: Prentice-Hall, 1996.

[31] Y. Zhou, X. Wang, X. Ye, J. Zhang, J. Zhou, and B. Chen, "Discrete-time sliding mode control with adaptive reaching law for rehabilitation exoskeleton," International Journal of Robust and Nonlinear Control, vol. 36, pp. 1820–1837, 2025.

[32] S. Sulaiman, F. Schetter, E. Shahabi, and F. Ficuciello, "A learning based impedance control strategy implemented on a soft prosthetic wrist in joint-space," Frontiers in Robotics and AI, vol. 12, p. 1665267, 2025.

[33] H.-H. Hsu, W.-K. Lee, and P.-L. Lee, "Designing an EEG signal-driven dual-path fuzzy neural network-controlled pneumatic exoskeleton for upper limb rehabilitation," International Journal of Fuzzy Systems, vol. 28, no. 3, pp. 982–1000, 2026.

[34] S. Abd-Elhaleem, A. H. El-Garawany, and M. El-Brawany, "Adaptive intelligent controller for a lower limb rehabilitation robot using QAOA-based online membership optimization," Scientific Reports, vol. 16, p. 10400, 2026.

[35] M. Kharrat and P. Mercorelli, “A comprehensive review of adaptive control for nonlinear systems with nonlinearities and faults using fuzzy logic and neural network techniques,” Mathematics, vol. 14, no. 8, p. 1256, 2026.

[36] S. Autsou, O. Dunajeva, A. Pentel, O. Shvets, and M. Roosileht, “Application of fuzzy logic for collaborative robot control,” Electronics, vol. 14, no. 20, p. 4029, 2025.

[37] J. G. Garcia, E. F. Luque, E. Romero, M. Parra, D. Suarez, V. E. Abarca, and D. A. Elias, “Assessment of artificial intelligence-based control algorithms to be implemented in an affordable transradial myoelectric prosthesis,” Scientific Reports, vol. 16, p. 14382, 2026.

[38] M. Chaucala-Gualotuña, D. De la Cruz-Guevara, J. Tobar-Quevedo, and M. Alban-Escobar, “Hand prosthesis with soft robotics technology and artificial intelligence for fine motor control,” Sensors, vol. 26, no. 5, p. 1423, 2026.

[39] Y. Çelik and U. Can, “Surface EMG-based hand gesture recognition using a hybrid multistream deep learning architecture,” Sensors, vol. 26, no. 7, p. 2281, 2026.

[40] S. Zhang, H. Zhou, R. Tchantchane, and G. Alici, “A co-located sEMG-pFMG dataset for hand gesture recognition under varying arm-position conditions,” Sensors, vol. 26, no. 14, p. 4626, 2026.

[41] R. Rodríguez Serrezuela, R. Sagaro Zamora, D. Milanés Hermosilla, A. E. Rivera Gomez, and E. Marañon Reyes, “Association of amputation-related clinical variables with subject-specific sEMG hand-gesture classification in transradial amputees: A comparative secondary analysis of CNN and convolutional vision transformer models,” Applied Sciences, vol. 16, no. 17, p. 8369, 2026.

[42] P. Tamilvanan, V. K. Elumalai, and B. Elumalai, “A comprehensive survey of machine learning algorithms in hand gesture recognition for myoelectric prosthetic control: Current trends, challenges and future directions,” Archives of Computational Methods in Engineering, vol. 33, no. 4, pp. 5839–5868, 2026.

[43] B. Abdikenov, D. Zholtayev, K. Suleimenov, N. Assan, K. Ozhikenov, A. Ozhikenova, N. Nadirov, and A. Kapsalyamov, “Emerging frontiers in robotic upper-limb prostheses: Mechanisms, materials, tactile sensors and machine learning-based EMG control: A comprehensive review,” Sensors, vol. 25, no. 13, p. 3892, 2025.

[44] J. Won and M. Iwase, “Highly responsive robotic prosthetic hand control considering electrodynamic delay,” Sensors, vol. 25, no. 1, p. 113, 2025.

[45] T. Zaim, S. Abdel-Hadi, R. Mahmoud, A. Khandakar, S. M. Rakhtala, and M. E. H. Chowdhury, “Machine learning- and deep learning-based myoelectric control system for upper limb rehabilitation utilizing EEG and EMG signals: A systematic review,” Bioengineering, vol. 12, no. 2, p. 144, 2025.

[46] A. Adetunla, C. Anulunko, T.-C. Jen, and C. K. Chan, “Integration of EMG and machine learning for real-time control of a 3D-printed prosthetic arm,” Prosthesis, vol. 7, no. 6, p. 166, 2025.

[47] C. Zhang, D. Zhou, Y. Fang, N. Kubota, and Z. Ju, “Surface EMG sensing and granular gesture recognition for rehabilitative pouring tasks: A case study,” Biomimetics, vol. 10, no. 4, p. 229, 2025.

[48] E. Aghchehli, M. Jabbari, C. Ma, M. Dyson, and K. Nazarpour, “Medium density EMG armband for gesture recognition,” Frontiers in Neurorobotics, vol. 19, p. 1531815, 2025.

[49] T. Donnelly, E. Seminati, and B. Metcalfe, “Approaches for retraining sEMG classifiers for upper-limb prostheses,” Frontiers in Neurorobotics, vol. 19, p. 1627872, 2025.

[50] D. Quadrelli, M. Canepa, D. Di Domenico, N. Boccardo, M. Chiappalone, and M. Laffranchi, “Advances in HD-EMG interfaces and spatial algorithms for upper limb prosthetic control,” Frontiers in Neuroscience, vol. 19, p. 1655257, 2025.

[51] I. Ben Abdallah, Y. Bouteraa, and A. Alotaibi, “A hybrid EMG–EEG interface for robust intention detection and fatigue-adaptive control of an elbow rehabilitation robot,” Scientific Reports, vol. 15, p. 40895, 2025.

8% Overall Similarity

The combined total of all matches, including overlapping sources, for each database.

Filtered from the Report

- Bibliography
- Quoted Text

Match Groups

204 Not Cited or Quoted 8%
Matches with neither in-text citation nor quotation marks

4 Missing Quotations 0%
Matches that are still very similar to source material

0 Missing Citation 0%
Matches that have quotation marks, but no in-text citation

0 Cited and Quoted 0%
Matches with in-text citation present, but no quotation marks

Top Sources

5% Internet sources
5% Publications
6% Submitted works (Student Papers)

Integrity Flags

0 Integrity Flags for Review

Our system's algorithms look deeply at a document for any inconsistencies that would set it apart from a normal submission. If we notice something strange, we flag it for you to review.

A Flag is not necessarily an indicator of a problem. However, we'd recommend you focus your attention there for further review.

Match Groups

204 Not Cited or Quoted 8%
Matches with neither in-text citation nor quotation marks

4 Missing Quotations 0%
Matches that are still very similar to source material

0 Missing Citation 0%
Matches that have quotation marks, but no in-text citation

0 Cited and Quoted 0%
Matches with in-text citation present, but no quotation marks

Top Sources

5% Internet sources
5% Publications
6% Submitted works (Student Papers)

Top Sources

The sources with the highest number of matches within the submission. Overlapping sources will not be displayed.

1	Internet	
dspace.bahria.edu.pk:8080		**<1%**
2	Student papers	
Higher Education Commission Pakistan on 2026-01-02		**<1%**
3	Student papers	
Higher Education Commission Pakistan on 2021-12-25		**<1%**
4	Student papers	
University of Gloucestershire on 2026-05-29		**<1%**
5	Internet	
www.mdpi.com		**<1%**
6	Internet	
semspub.epa.gov		**<1%**
7	Internet	
mdpi-res.com		**<1%**
8	Student papers	
Bahria University, Islamabad on 2025-10-15		**<1%**
9	Publication	
V N Jayasankar, Nisha B Kumar, U Vinatha. "Enhancement of load voltage compe...		**<1%**
10	Internet	
cours-examens.org		**<1%**

11 Internet

ebin.pub <1%

12 Publication

Ricardo Rojas-Galván, Josué A. Romero-Moreno, Roberto V. Carrillo-Serrano, José … <1%

13 Student papers

University of Nottingham on 2026-04-26 <1%

14 Student papers

Glasgow Caledonian University on 2025-09-01 <1%

15 Publication

Hassan Yousefi, Heikki Handroos, Reza Dovali, Azita Soleymani. "Designing Fuzzy … <1%

16 Student papers

Lahore Garrison University-Lahore. on 2025-11-04 <1%

17 Internet

vdoc.pub <1%

18 Student papers

Universidad Nacional de Colombia on 2017-11-24 <1%

19 Internet

link.springer.com <1%

20 Internet

dokumen.pub <1%

21 Publication

Kaitian Luo, Shenhong Lei, Chaoqing Li, Yi Li. "Anomaly Detection Based on Hybri… <1%

22 Publication

Shun-Yuan Wang, Chwan-Lu Tseng, Foun-Yuan Liu, Jen-Hsiang Chou, Chun-Liang … <1%

23 Internet

tudr.thapar.edu:8080 <1%

24 Student papers

University of Edinburgh on 2013-08-14 <1%

25 Publication

Qifu Wang, Chenchen Jiang, Jun Ning, Liying Hao, Yong Yin. "Fuzzy Course Trackin… <1%

26 Publication

Advances in the Biomechanics of the Hand and Wrist, 1994. <1%

27 Student papers

University of Technology on 2026-08-19 <1%

28 Internet

cyberleninka.org <1%

29 Internet

prr.hec.gov.pk <1%

30 Publication

D.W. Repperger. "An adaptive learning system yielding unbiased parameter esti… <1%

31 Internet

core.ac.uk <1%

32 Internet

etd.astu.edu.et <1%

33 Internet

scitepress.org <1%

34 Publication

Heng Liu, Yongping Pan, Jinde Cao. "Composite Learning Adaptive Dynamic Surfa… <1%

35 Student papers

National Institute of Technology, Rourkela on 2014-05-30 <1%

36 Student papers

University of Glasgow on 2026-08-10 <1%

37 Student papers

Vellore Institute of Technology on 2026-06-09 <1%

38 Internet

pmc.ncbi.nlm.nih.gov <1%

39 Internet

www.mate.tue.nl <1%

40 Publication

C.W. de Silva. "Mechatronic Systems - Devices, Design, Control, Operation and Mo... <1%

41 Internet

etd.repository.ugm.ac.id <1%

42 Internet

hdl.handle.net <1%

43 Internet

www.docstoc.com <1%

44 Internet

www.haya.nuem.nagoya-u.ac.jp <1%

45 Publication

Dissanayake Ralalage, Anushka Madushan. "Optimal Energy Management and C... <1%

46 Publication

Haojian Xu, P.A. Ioannou. "Robust adaptive control for a class of mimo nonlinear ... <1%

47 Student papers

University of East London on 2026-05-07 <1%

48 Student papers

University of Sheffield on 2022-09-10 <1%

49 Internet

journals.tums.ac.ir <1%

50 Internet

www.slideshare.net <1%

51 Student papers

Manipal University on 2025-11-16 <1%

52 Student papers

University of Malaya on 2010-11-25 <1%

53 Internet

ksascholar.dri.sa <1%

54 Publication

A. Datta, P.A. Ioannou. "Performance analysis and improvement in model referen... <1%

55 Student papers

University of Sydney on 2016-05-08 <1%

56 Internet

repository.aaup.edu <1%

57 Publication

A. Biswas. "Silk cocoon grading by fuzzy expert systems", Soft computing in textil... <1%

58 Publication

Paul Tucan, Oana-Maria Vanta, Calin Vaida, Mihai Ciupe et al. "Fuzzy Adaptive Co... <1%

59 Publication

Tavakoli, Mahmoud, Baptiste Enes, Joana Santos, Lino Marques, and Anibal T. de ... <1%

60 Student papers

Universiti Teknologi Malaysia on 2013-10-28 <1%

61 Publication

Akshya Swain. "Control Systems Engineering Principles and Practice - Classical an... <1%

62 Student papers

Indian Institute of Technology Guwahati on 2015-10-09 <1%

63 Student papers

Teaching and Learning with Technology on 2026-04-05 <1%

64 Student papers

The University of Manchester on 2025-08-31 <1%

65 Student papers

University of Newcastle upon Tyne on 2008-09-08 <1%

66 Internet

dspace.lboro.ac.uk <1%

67	Internet	
dspace.mit.edu		<1%
68	Internet	
esource.dbs.ie		<1%
69	Internet	
etd.aau.edu.et		<1%
70	Internet	
sure.sunderland.ac.uk		<1%
71	Internet	
www.coursehero.com		<1%
72	Publication	
Hamamoto, K.. "Iterative feedback tuning of controllers for a two-mass-spring sy...		<1%
73	Publication	
Terry, Jonathan Spencer. "Adaptive Control for Inflatable Soft Robotic Manipulato...		<1%
74	Student papers	
University of Nottingham on 2026-05-15		<1%
75	Student papers	
University of Wollongong on 2025-03-04		<1%
76	Publication	
Yasir Mohammed Ali Saeed, Mohammed Sabah Jarjees. "Chapter 16 A Review of H...		<1%
77	Internet	
downloads.hindawi.com		<1%
78	Internet	
uwspace.uwaterloo.ca		<1%
79	Publication	
Mohamed Fawzy El-Khatib, M. Abdelfattah, Mohamed M. El-Sotouhy, S. Shaaban, ...		<1%
80	Publication	
Sameh Abd-Elhaleem, Ahmed Hamdy El-Garawany, Mohamed El-Brawany. "Adapt...		<1%

81 Publication

Steffen, Nathan R.. "Fuzzy Ordinary Differential Equations for Intelligent Aerospa... <1%

82 Internet

eprints.kingston.ac.uk <1%

83 Internet

www.minhang.cc <1%

84 Student papers

Heriot-Watt University on 2015-08-21 <1%

85 Student papers

King Fahd University for Petroleum & Minerals on 2026-07-02 <1%

86 Publication

Salim Labiod, Thierry Marie Guerra. "Direct adaptive fuzzy control for a class of M... <1%

87 Internet

arxiv.org <1%

88 Internet

controlengineers.ir <1%

89 Internet

d197for5662m48.cloudfront.net <1%

90 Internet

docslib.org <1%

91 Internet

etheses.whiterose.ac.uk <1%

92 Internet

www.mathworks.com <1%

93 Publication

özdemir, Mehmet Akif. "Image-Based Representations of Physiological Signals: D... <1%

94 Publication

"Mechanism Design for Robotics", Springer Science and Business Media LLC, 2027 <1%

95 Publication

A.D. Cheok, N. Ertugrul. "Use of fuzzy logic for modeling, estimation, and predicti… <1%

96 Publication

Enzo Romero, Jose G. Garcia, Magno Parra, Sebastian Caballa et al. "An Affordable… <1%

97 Student papers

Higher Education Commission Pakistan on 2026-07-30 <1%

98 Publication

Liu, Xinru. "Topics in Thompson Sampling and Sparse Bayesian Machine Learning… <1%

99 Student papers

Nazarbayev University on 2026-04-11 <1%

100 Publication

Prashant Prakash, Mamta Juneja, Archita, Harleen Kaur, Nirmal Raj Gopinathan, … <1%

101 Publication

R.R. Yager, D.P. Filev, T. Sadeghi. "Analysis of flexible structured fuzzy logic contro… <1%

102 Publication

Shen Zhang, Hao Zhou, Rayane Tchantchane, Gursel Alici. "A Co-Located sEMG-pF… <1%

103 Student papers

Universiti Kuala Lumpur on 2026-06-09 <1%

104 Student papers

University of Auckland on 2025-07-09 <1%

105 Student papers

University of Cape Coast on 2026-05-05 <1%

106 Student papers

University of Essex on 2026-08-25 <1%

107 Student papers

University of Hertfordshire on 2026-01-05 <1%

108 Student papers

University of Leeds on 2025-05-01 <1%

109 Student papers

University of Queensland on 2016-05-27 <1%

110 Student papers

University of Sheffield on 2023-05-11 <1%

111 Student papers

University of South Wales - Pontypridd and Cardiff on 2026-01-29 <1%

112 Publication

Zhiqiang Li, Kun Luo, Liang Tao, Yan Zhou. "Adaptive PID Control of the Drive Syst… <1%

113 Internet

conferences.lib.unb.ca <1%

114 Publication

da Silva Almeida, João Pedro. "Energy Efficiency Management Module", Universid… <1%

115 Internet

eprints.utas.edu.au <1%

116 Internet

era.library.ualberta.ca <1%

117 Internet

folk.ntnu.no <1%

118 Internet

gaines.library.uvic.ca <1%

119 Internet

ijai.iaescore.com <1%

120 Internet

ir.vistas.ac.in <1%

121 Internet

kclpure.kcl.ac.uk <1%

122 Internet

scholarhub.unimas.my <1%

123 Internet

waseda.repo.nii.ac.jp <1%

124 Internet

www.di3.drexel.edu <1%

125 Internet

www.unb.ca <1%

126 Publication

Fuad E. Alsaadi, Njud S. Alharbi. "Deep neural network-integrated finite-time faul… <1%

127 Student papers

Imperial College of Science, Technology and Medicine on 2025-06-13 <1%

128 Publication

J.-S.R. Jang. "ANFIS: adaptive-network-based fuzzy inference system", IEEE Transa… <1%

129 Student papers

University of Derby on 2014-09-14 <1%

130 Publication

Yongkun Lu. "Adaptive-Fuzzy Control Compensation Design for Direct Adaptive F… <1%

131 Student papers

BBPlugin on 2026-08-21 <1%

132 Student papers

EuroCollege Examenbureau on 2026-06-12 <1%

133 Publication

Nazmul Siddique. "Intelligent Control", Springer Science and Business Media LLC, … <1%

134 Student papers

Robert Kennedy College on 2026-08-25 <1%

135 Student papers

University of Hull on 2020-05-12 <1%

136 Publication

William S. Levine. "Control System Fundamentals", CRC Press, 2019 <1